

# Flexoelectricity and surface ferroelectricity of water ice

**Authors:** X. Wen<sup>1,3</sup>, Q. Ma<sup>1</sup>, A. Mannino<sup>4,5</sup>, M. Fernandez-Serra<sup>4,5</sup>, S. Shen<sup>1\*</sup>, G. Catalan<sup>2,3\*</sup>

## **Affiliations:**

<sup>1</sup>State Key Laboratory for Strength and Vibration of Mechanical Structures, School of Aerospace Engineering, Xi'an Jiaotong University, Xi'an, China.

<sup>2</sup>ICREA—Institutio Catalana de Recerca i Estudis Avançats, Passeig Lluís Companys 23, Barcelona, Catalonia

<sup>3</sup>Institut Catala de Nanociencia i Nanotecnologia (ICN2), CSIC and The Barcelona Institute of Nanoscience and Technology (BIST), Campus Universitat Autònoma de Barcelona, Bellaterra, Catalonia.

<sup>4</sup>Physics and Astronomy Department, Stony Brook University, Stony Brook, New York 11794-3800, United States

<sup>5</sup>Institute for Advanced Computational Science, Stony Brook University, Stony Brook, New York 11794-3800, United States

\*Corresponding author. Email: sshen@mail.xjtu.edu.cn; gustau.catalan@icn2.cat

## **Abstract:**

The phase diagram of ice is complex and contains many phases, but the most common (frozen water at ambient pressure, also known as Ih ice) is a non-polar material despite individual water molecules being polar. Consequently, ice is not piezoelectric and cannot generate electricity under pressure. On the other hand, the coupling between polarization and strain gradient (flexoelectricity) is universal, so ice may in theory generate electricity under bending. Here we report the experimental demonstration that ice is flexoelectric, finding a coefficient comparable to that of ceramics such as SrTiO<sub>3</sub> or TiO<sub>2</sub>. Additionally, and unexpectedly, the sensitivity of flexoelectric measurements to surface boundary conditions has also revealed a ferroelectric phase transition around  $163 \pm 5\text{K}$  confined in the near-surface region of the ice slabs. The electromechanical properties of ice may find applications for low-cost transducers made in-situ in cold and remote locations, but perhaps more important are the consequences for natural phenomena involving ice electrification. In particular, we have calculated the flexoelectric polarization generated in collisions between ice and graupel particles, which reproduces the experimentally reported results for contact electrification in such events, known to cause electrification in storm clouds.

## Main Text:

Ice, formed by hydrogen bonding of water molecules ( $\text{H}_2\text{O}$ ), is one of the most widespread and abundant solids on earth. Manifesting as snowflakes, frosts, and glaciers in nature, it plays an essential role in geology, meteorology, and astronomy[1]. Moreover, even liquid water is ice-like when nano-confined or at the interface with solids[2], which renders the physics of ice also relevant to life science and electrochemistry[3,4]. Despite the ongoing interest and large body of knowledge on ice[5], new phases[6,7] and anomalous properties[8] continue to be discovered, suggesting that our understanding of this ubiquitous material is far from complete.

An interesting open question concerns the electromechanical properties of ice. Despite the polarity of individual water molecules, common ice  $\text{I}_h$  is not piezoelectric[5], due to the geometric frustration introduced by the so-called Bernal-Fowler rules[1,5]: two hydrogen protons must be adjacent to each oxygen atom, but there can only be one hydrogen proton between two oxygen atoms. As a result, in contrast to the oxygen atoms, which are arranged in a hexagonal lattice, the hydrogen atoms do not exhibit long-range order[5], resulting in randomly oriented water dipoles and thus no macroscopic piezoelectricity. Yet ice is known to generate electricity under mechanical stress in nature. For example, ice collisions and fractures cause electrifications in clouds[9,10] and polar regions[11,12]. The underpinning electromechanical mechanism of these natural phenomena, however, remains elusive.

In this context, we bring our attention to flexoelectricity, a coupling between electrical polarization and strain gradients that, contrary to piezoelectricity, can exist in materials of any symmetry[13,14]. In theory, then, it may also exist in ice. Yet, despite a growing awareness of flexoelectricity and its consequences in other materials[15-20], the flexoelectricity of ice remains unknown. In this article we report its measurement and examine some of its repercussions.

We have prepared ice capacitors by freezing at ambient pressure a layer of ultrapure water (milli-Q, resistivity  $>10 \text{ M}\Omega\cdot\text{cm}$ ) between two gold-coated aluminum electrodes (Fig. 1a and b). Our samples are polycrystalline (mean grain size  $\sim 77 \mu\text{m}$ ) and are at ordinary  $\text{I}_h$  phase with a preferential orientation of [001] throughout the experimental temperature range, as verified by X-ray diffraction and Raman spectroscopy (See Fig. S1 in Supplemental Material[21]). Piezoelectric measurements confirm the non-piezoelectric nature of our ice samples (See Fig. S2 in Supplemental Material[21]).

To measure ice flexoelectricity, we have used a dynamic mechanical analyzer (DMA) to deliver an oscillating three-point bending deformation to the ice capacitors (See Fig. S3 in Supplemental Material [21]). The vertical deflection (measured by a displacement sensor) and the bending-induced charge (collected by a charge amplifier) are synchronously recorded by an oscilloscope, and are then used to calculate strain gradients and polarization respectively. Fig.

1c plots the Fourier-filtered first-harmonic data of the applied displacement and the induced charge. The induced polarization, measured as a function of applied a.c. strain gradient, is plotted in Fig. 1d. It shows the linear dependence expected for a flexoelectric material. The slope of the linear fit (1.65 nC/m) represents the effective flexoelectric coefficient  $\mu_{13}^{eff}$  of ice Ih. The results shown in Fig. 1c and d were obtained at 237 K, a temperature well below melting, and around which ice flexoelectricity was found to be relatively temperature-independent and far from any anomaly. However, there are anomalies both at higher temperatures (>248 K) and lower ones (<203K), which we discuss next.

The temperature dependence of flexoelectricity was measured in the range between 143 K and 273 K simultaneously with the mechanical response of the ice slabs. Representative results for three samples are plotted in Fig. 2a. Three distinct regimes can be identified. Above 248 K, flexoelectricity starts to increase, and the phase angle between strain gradient and induced polarization shifts away from 0 deg (Fig. 2a and b), accompanied by the onset of mechanical creep (Fig. 2c). These anomalies coincide with the surface transition to pre-melting quasi-liquid layers (QLL) [22-25], with a reported wide critical temperature range from 213 K to 253 K[26-31] (see Fig. S4 in Supplemental Material for direct comparison between reported QLL results and our measurements[21]). The QLL of ice contains mobile ions that facilitate charge transport[24] and grain-boundary sliding[32], consistent respectively with the observed increase of flexoelectricity[16] (and shift its phase angle from capacitive to conductivity-dominated response[33]), and with the mechanical softening above 248 K (Fig 2). The results therefore indicate that the flexoelectric and mechanical anomalies above 248 K can be attributed to the onset of pre-melting. To ensure a creep-free initial condition, in fact, measurements were always started from about 223 K (i.e. below the QLL temperature) rather than 273 K, then cooled down to 143 K (See Fig. S5 in Supplemental Material[21]), finally followed by heating measurements all the way up to 273 K (Fig. 2 and Fig. 3).

In the temperature range between 203 K to 248 K, the flexoelectric coefficient was found to be quite constant around 1~3 nC/m. This is in the same range as dielectric ceramics such as SrTiO<sub>3</sub>[34], TiO<sub>2</sub>[16], or PbZrO<sub>3</sub>[35]. Flexoelectricity is proportional to dielectric permittivity [13,14], and this result is consistent with the relatively high dielectric constant of bulk ice,  $\epsilon_r \sim 100$ [5]. The flexocoupling coefficient (flexoelectric constant divided by dielectric permittivity) is  $\sim 2$  volts, which also agrees with the 1-10V expected range for intrinsic flexoelectricity in solids[14]. We therefore conclude that  $2 \pm 1$  nC/m is the intrinsic value of the flexoelectric coefficient of ice.

Below 203 K, however, the flexoelectric coefficient begins to grow again, reaching a peak value of  $\sim 7.6$  nC/m at around 163 K  $\pm 5$  K (Fig. 2a). Such a temperature dependence of

flexoelectricity has only been observed before in ceramic materials with ferroelectric or antiferroelectric phase transitions[35-37], so a question emerges: is the flexoelectric anomaly of ice related to a ferroelectric phase transition?

Ice can become ferroelectric in some conditions. Doping bulk ice with alkali hydroxides causes proton rearrangement and transform ice-Ih to ferroelectric ice-XI at 72 K[1]. On the other hand, the flexoelectric peak of our ice slabs indicates a critical temperature  $\sim 100$  K higher than the Curie temperature of bulk doped ice. Moreover, the mechanical response of our samples (Fig. 2c) shows no sign of any structural phase transition, nor do the Raman measurements as a function of temperature of our samples show any change of symmetry (See Fig. S1 in Supplemental Material[21]), and the maximum bending-induced stress in the surfaces of our sample is  $\sim 0.005$  Gpa (See Fig. S6 in Supplemental Material[21]), two orders of magnitude smaller than the minimum stress that can cause a phase transition in ice [38,39]. The flexoelectric peak at  $\sim 163$  K therefore cannot be attributed to a bulk or strain-induced ferroelectric transition.

On the other hand, ultra-thin films of ice grown on platinum substrates have been reported to become ferroelectric[40,41] around 163 K $\sim$ 175 K[41,42], which is similar to the temperature range of our flexoelectric anomaly. Although our ice samples are thick ( $\sim 2$  mm) and have gold electrodes instead of platinum, the similarity of critical temperatures is tantalizing. A unique feature of flexoelectricity is that it contains comparable contributions from the bulk and the surface, irrespective of the sample thickness[43,44]; even in bulk samples, surfaces can still determine the magnitude and even the sign of the total flexoelectric coefficient[16,33,45,46]. Given the inherent contribution of surfaces to total flexoelectricity, the lack of evidence for a bulk phase transition, and the known existence of ferroelectricity in thin films with a similar critical temperature as that of our flexoelectric peak, we hypothesize that the origin of the flexoelectric peak is a ferroelectric phase transition confined within the near-surface region of our samples. Skin layers with distinct properties are common in oxide electroceramics[47,48], and ice itself is already known to show an interfacial QLL transition below the bulk melting temperature[25], so it is not unreasonable to expect the surface of ice to have its own ferroelectric transition with a  $T_c$  different from the bulk. Next, we examine this hypothesis in closer detail.

In a slab with opposite polar surfaces, surface piezoelectricity can contribute to effective flexoelectricity as depicted in Fig. 3a: under bending, the different signs of the strain (compressive on one side, tensile on the other) cause a difference in polarization, which is additional to the bulk flexoelectricity. Within this model, and assuming the piezoelectric coefficient of ice XI for the interfacial layers, we expect their thickness to be 17.5 nm (See S3 and S4 in Supplemental Material[21]). It has been suggested<sup>[49]</sup> that the free surface of ice

remains polar at all temperatures below the premelting point ( $\sim 248\text{K}$  in our sample), but such a result cannot explain the observed phase transition at  $163\text{K}$ . The difference is likely related to the presence of the electrodes in the ice capacitors. To test this hypothesis, we have replaced the Au electrodes with other metals. Measurements on three different Pt/ice/Pt capacitors are presented in Fig. 3b, showing similar temperature dependence of flexoelectricity but a larger maximum of  $\sim 15\text{ nC/m}$  at  $\sim 158\text{ K}$  ( $\pm 5\text{ K}$ ) (see Fig. S8 in Supplemental Material for phase angle[21]). The flexoelectric peak of ice with Pt electrodes is larger than that with Au electrodes (Fig. 3b). The calculated thickness of the piezoelectric interfacial layers in this case is  $31.3\text{ nm}$  (See S4 in Supplemental Material[21]).

The electrode effect is consistent with Sugimoto's explanation for the origin of ferroelectricity in thin films[41], whereby interfacial ferroelectric ordering is triggered by electron transfer from the surface to the electrode in order to equilibrate chemical potentials. The work function  $\phi$  of gold ( $\sim 5.1\text{ eV}$ )[50] is higher than that of ice ( $\sim 4.4\text{ eV}$ )[51,52], and the work function of Pt ( $\sim 5.65\text{ eV}$ )[50] is higher yet, resulting in a bigger poling field, consistent with the observed higher flexoelectric anomaly. Conversely, the work-function of Al (about  $4.28\text{ eV}$ [50]) is smaller than those of Au and Pt and very close to that of ice. The interfacial field between ice and Al is therefore very small, and indeed the ice capacitors with Al electrodes show no visible flexoelectric peak (Fig. 3b). In Fig. 3c we have plotted the peak value of the flexoelectric coefficient as a function of the electrode work-functions, showing a direct proportionality.

We have further studied the effect of the pre-poling field on the flexoelectric coefficient and found a butterfly hysteresis loop (Fig. 3d). Note that each point of the loop was measured after switching off the biasing voltage, meaning that the hysteresis is not due to a leakage artifact[53]. The measurement of hysteresis, which is a defining feature of ferroelectricity, had in fact been elusive in ice prior to the present work, due to the difficulty of depositing non-shortening electrodes in ultra-thin films such as Sugimoto's. Besides supporting the existence of interfacial ferroelectricity, therefore, the present results also showcase how flexoelectricity can be utilized to explore interfacial properties while retaining the convenience of bulk samples.

To further understand the microscopic origin of the surface phase transition, we also computed the surface free energies of ice-metal interfaces, using density functional theory. It has been previously shown, both experimentally and theoretically[40,54-56], that metallic Au, Pt, and Pd [111] surfaces affect the dipole orientation of  $\text{H}_2\text{O}$  at the interface. Although our samples are polycrystalline, X-ray diffraction (See Fig. S1 in Supplemental Material[21]) shows that the predominant out-of-plane orientation of the ice grains is hexagonal [001], and cubic [111] for the electrodes, so we assume these orientations in the calculations. We have

computed the free energies of two interfaces: ferroelectric ice-XI on Au[111], with the ice-XI dipole pointing towards the metal surface (Fig. 4a), and common ice-Ih on Au[111], without ordered dipoles (Fig. 4b). We then compare the difference in cohesive energy between these two systems with the cohesive energy difference between bulk ice XI and bulk ice Ih without the Au slab. The result is that the Au interface enhances the stability of the polar phase by 140 meV.

When the interfacial energy gain is distributed among all the molecules in the interfacial layer and subtracted from the Helmholtz free energy of ice XI (Fig. 4c), the calculations predict that the Curie temperature should shift to the observed phase transition temperature of 163 K for a skin layer thickness of  $\sim 14.9$  nm (see Fig 4d, and S5 in Supplemental Material[21]), which is comparable to the experimental estimate of 17.5 nm. We have also repeated the calculations replacing Au with Pt, finding that the stability of the proton ordered (XI) interface relative to the proton disordered (Ih) interface is enhanced by 307 meV. At the observed phase transition temperature of 158 K (for the ice capacitors with Pt electrodes), this corresponds to a ferroelectric skin layer thickness of 35.1 nm (Fig. 4d), in good agreement with the experimental estimate of 31.3 nm. Further details of the calculations are provided in the Supplemental Material[21].

Lastly, we examine some consequences of ice flexoelectricity in nature. It has long been known that collisions between small ice particles and large graupel particles cause charge separation in clouds, and eventually cause lightning [9,10,24,57]. The transferred charge carriers are known to be ions residing in the QLL on ice surfaces[24] (See S6 in Supplemental Material [21]), but the force that drives ion transfer between chemically identical particles remains ambiguous[58]. Current explanations invoke additional assumptions to break the symmetry between two bodies (See S7 in Supplemental Material[21]), such as gradients of temperature[57,59], electric potential[60-62], and surface ion concentration[63,64]. But these explanations do not adequately depict the entirety of ice electrifications, as charge transfer has been measured even in the absence of these required preconditions[65-72]. In this context, strain gradients can provide a way forward. They are inevitable in collision deformations, and they are known to inherently break spatial symmetry, resulting in skewed thermodynamic potentials[15]. The connection between flexoelectricity and triboelectricity has been suggested[73-77] and measured in ferroelectrics[78]. In view of these considerations, we examine whether collision-induced flexoelectricity can, without additional parameters, account for the contact electrification of ice.

We have calculated the flexoelectric polarization beneath the surface of the larger graupel particle, calculated using elastic Hertzian model for contact deformations with our measured

flexoelectric coefficient and typical parameters of ice-collisions events (see S8 and S9 in Supplemental Material for details [21]). The largest induced flexoelectric polarization is  $\sim 10^{-4}$  C/m<sup>2</sup> at the interface (See Fig. S12a in Supplemental Material [21]). This surface polarization creates an electric field (aka the depolarizing field, Fig. 5a) of the order of  $10^5$  V/m, which is comparable with the external electric field used in previous studies to trigger CE ( $0\sim 10^5$  V/m)[62,79,80]. This field skews the double well of potential energy at the interface between the two ice particles (Fig. S12b), effectively becoming the driving force for redistributing the surface ions[81-83] across the contact interface[84-86]. Our model predicts an amount of charge transfer in the order of  $10^0\sim 10^2$  fC per collision (Fig. 5b), comparable with the charge transfer (10~65 fC) required for the culmination of lightning[10,87]. Furthermore, as shown in Fig. 5c and d, this model reproduces the dependence of charge on particle size and colliding velocity reported in previous experiments performed in cloud-simulating conditions[65-72]. Besides the quantitative match in magnitude, the reported elusive sign reversal of charge transfer direction upon temperature increase [10,57,65] can also be explained by the phase angle reversal of flexoelectricity near the melting point (Fig. 2b). These agreements with ice experiments highlight the need to incorporate flexoelectricity into the analysis of ice electrification.

In conclusion, water ice is both flexoelectric and, at its surface, ferroelectric. The interfacial ferroelectricity of ice has been observed below  $\sim 160$ K, while its flexoelectricity makes ice electromechanically active at all temperatures, and will therefore participate in any natural process involving mechanical deformations of ice or ice-like interfacial water.

## Materials and Methods

**Preparation of electrodes.** Aluminum foils with a thickness of 15  $\mu\text{m}$  (BS-QT-027, Biosharp) were cut into strips with a length of 100 mm and width of 5 mm, which were then chemically cleaned by acetone, ethanol, and ultrapure water sequentially. To study the electrode dependence of ice flexoelectricity, we coated a gold or platinum layer of  $\sim 100$  nm on the surface of cleaned Al foils with an Ion Sputter Coater (MC1000, HITACHI). Copper wires were attached to the foils by a drop of silver paste (948-06G, HumiSeal), which was then solidified at 373 K for half-hour. To check the conductivity of the adhesion, we used a multimeter to measure the resistance from the copper wire to the aluminum foil. When the resistance is less than 1 Ohm, the electrodes were used for the following steps.

**Preparation of water and ice capacitors.** Ultrapure water produced by a water purification system (Sistema Milli-Q Advantage A10) was used as the mother material for fabricating pure ice. Water was degassed in a vacuum drying oven (DZF-6050, ShanghaiYiheng) at room temperature until no air bubbles were generated. Two pieces of cleaned aluminum foil (or sputtered with Au or Pt) were placed horizontally on the dynamic mechanical analyzer with a vertical air gap. The air gap was engineered by placing two ceramic bars on the left and right sides of the clamps as shown in Fig. 1a. Degassed ultrapure water was then added into the air gap between foils by a plastic dropper. Thanks to the surface tension, the water could maintain a good shape instead of spreading to the left and right sides. With two electrodes and one layer of water in between, a water capacitor was obtained (Fig. 1a). Then, the water capacitor was frozen at 253 K for an hour and a half to obtain the ice capacitor. By cutting the redundant electrodes on left and right sides, we had an ice capacitor ready for flexoelectric characterizations (Fig. 1b). The thickness of the ice capacitors was measured by a vernier caliper in the temperature box after the flexoelectric measurements, which ranges from 1.8mm to 2.2mm.

**Structural characterizations.** The ice surface (Fig. S1a) was imaged under an optical microscope (NIKON ECLIPSE LV100D) with a temperature chamber (Linkam, HFS600E-PB4). Raman spectrum (Fig. S1c) was measured by a confocal Raman spectrometer (Witec Alpha300R) with the same Linkam chamber. The laser wavelength, power density, and grating were 532 nm, 8 mW and 600 lines/mm<sup>-1</sup> respectively. X-ray diffraction patterns (Fig. S1d) were measured by a Diffractometer (X'pert Pro MPD Malvern-Panalytical) with a low-temperature chamber from Anton Paar (TTK600). The top electrode of the ice capacitor, grown in-situ in the temperature chamber using the same method described above, was removed from ice to enable these measurements.

**Flexoelectric characterizations.** A dynamic mechanical analyzer (Electroforce 3200, TA



Instruments) was used to apply an oscillating 3-point bending deformation, which was recorded by a High Accuracy Displacement Sensor (HADS) embedded in the DMA. To reduce 1/f noise from the environment, relatively high drive frequencies (10~17 Hz) of the dynamic force were used, which is still far from the resonant frequency and so the loading can be regarded as a quasi-static condition. A small static force (typically -1.25N) was applied simultaneously to hold the sample in place.

The AC displacement  $\delta$  at the sample's center measured by the HADS is converted to the average strain gradient across the electrode area by[34]

$$\overline{\frac{\partial \varepsilon_{11}}{\partial x_3}} = \frac{12\delta}{L^3} (L - a), \quad (1)$$

where  $a$  is the half-length of the electrodes,  $L$  is the distance between two bottom ceramic bars. In our experiments,  $L$  and  $a$  are 30mm and 15mm respectively. The bending-induced electric charge was converted by an amplifier (2692, Brüel & Kjær) to a voltage signal by a charge gain of 100mV/pC, which was then recorded with the bending displacement synchronously by an oscilloscope (MDO3104, Tektronix). The measured charge  $Q$  was converted to the average electric polarization across the electrode area along the thickness direction by

$$\overline{P}_3 = \frac{Q}{A}, \quad (2)$$

where  $A$  is the area of the electrodes and equal to 30mm\*5mm in our experiments. To exclude the environmental interferences, we performed the Fourier transformation on the recorded displacement  $\delta$  and charge  $Q$  and used the first-harmonic signal for the calculations in equation (1) and (2). With the measured strain gradient and polarization, the effective flexoelectric coefficient is calculated by

$$\mu_{13}^{eff} = \overline{P}_3 / \overline{\frac{\partial \varepsilon_{11}}{\partial x_3}} \quad (3)$$

To further make sure what we are measuring is flexoelectricity rather than the environmental noise, we applied different forces to the sample and measured the corresponding induced charge. By doing a linear regression of the relationship between strain gradients and polarization, we extracted the slope value as the effective flexoelectric coefficient and the standard error value as the error bar (Fig. 1d). Every data point in Fig. 2a, Fig. 3b and Fig. S4, including its mean value and error bar, is calculated by such a linear regression.

Temperature-dependent measurements were achieved by competitive action of a resistive heater and a liquid N<sub>2</sub> bath. We started the flexoelectric measurements at ~223 K, well below the temperature at which ice-pre-melting and creeping plastic deformation can occur, but still well above the ferroelectric transition of the surface layer. From that temperature, we measured on cooling down to 143 K, followed by heating measurements all the way up to 273 K. To

avoid the influence of the pyroelectric effect or any other interference, each measurement was performed at a fixed temperature instead of sweeping the temperature with a constant strain gradient. The temperature interval between each flexoelectric measurement was set to  $\sim 5$  K and the flexoelectric coefficient at each temperature was measured by doing the least squares regression of the polarization as a function of strain gradient for five different applied strain gradients.

**Ab Initio Simulations.** We used the siesta code[88,89] to perform DFT calculations within the generalized gradient approximation (GGA) to the exchange and correlation (XC) functional. The calculations use a combination of PBE[90] and vdW-DF(PBEx)[91,92] functionals. These density functionals have previously been shown to give good results for the bulk XI-Ih phase transition[93,94]. Relaxations are done using the same combination of parameters as described in[94]. For the free energy calculations which include the nuclear quantum effects[93,95], the vibrational modes are calculated using the frozen phonon approximation. We only compute the phonons for the bulk ices, and add to the free energy the classical energy of the ice-Au[111] interface. The proton order-to-disorder phase transition temperature is determined from the Helmholtz Free energy at zero pressure. We account for nuclear quantum effects in the bulk ices within the quasi-harmonic approximation, with details provided in S5(B) in Supplemental Material[21]. The main modification to the free energies of the bulk ices in this work arises from accounting for the zero-temperature interfacial binding energy contribution to the cohesive energy of ice. The computation of this energy is described in S5(A) in Supplemental Material [21].

**Acknowledgments:** We thank J. Liu for her code to process the experimental data, N. Domingo, D. Pesquera, M. Stengel for useful discussions, and P. Vales, J. M. Caicedo, D. Pesquera, S. Ganguly, J. Padilla for the technical support. This project is funded by the Spanish Ministry of Economy, Industry and Competitiveness (projects MAT2016-77100-C2-1-P), the Catalan AGAUR agency (project: 2017-SGR-579), and the National Natural Science Foundation of China (Grant No. 12090030). ICN2 is funded by the CERCA programme/Generalitat de Catalunya and by the Severo Ochoa programme (SEV-2017-0706). X.W. acknowledges the support from the China Scholarship Council and Juan de la Cierva fellowship. M.F.-S. and A.M. were funded by the U.S. Department of Energy, Office of Science, Basic Energy Sciences, under Award No. DE-SC0019394, as part of the CCS Program.

**Author contributions:** G.C. conceived the idea and coordinated this work. G.C. and X.W. designed the experiments. X.W. and Q.M. performed the experiments under the supervision of

G.C. and S.S., A.M. and M.F-S. performed the *ab initio* calculations and associated data modeling. X.W. performed the calculations for the electrification analysis. X.W. and G.C. wrote the manuscript with the input from all the other authors. All authors discussed the results and commented on the manuscript.

**Competing interests:** Authors declare that they have no competing interests.

**Data and materials availability:** All data are available in the main text or the supplementary materials

## References and Notes

- [1] T. Bartels-Rausch, V. Bergeron, J. H. E. Cartwright, R. Escribano, J. L. Finney, H. Grothe *et al.*, *Reviews of Modern Physics* **84**, 885 (2012).
- [2] L. Fumagalli *et al.*, *Science* **360**, 1339 (2018).
- [3] P. Ball, *Chem Rev* **108**, 74 (2008).
- [4] Y.-H. Wang *et al.*, *Nature* **600**, 81 (2021).
- [5] V. F. Petrenko and R. W. Whitworth, *Physics of ice* (OUP Oxford, 1999).
- [6] V. Kapil, C. Schran, A. Zen, J. Chen, C. J. Pickard, and A. Michaelides, *Nature* **609**, 512 (2022).
- [7] A. Rosu-Finsen, M. B. Davies, A. Amon, H. Wu, A. Sella, A. Michaelides, and C. G. Salzmann, *Science* **379**, 474 (2023).
- [8] P. Xu, B. Cui, Y. Bu, H. Wang, X. Guo, P. Wang, Y. R. Shen, and L. Tong, *Science* **373**, 187 (2021).
- [9] S. Reynolds, M. Brook, and M. F. Gourley, *Journal of Atmospheric Sciences* **14**, 426 (1957).
- [10] C. J. P. A. E. Saunders, 335 (2008).
- [11] D. V. Thiel, *Cold Regions Science and Technology* **21**, 49 (1992).
- [12] D. A. Fifolt, V. F. Petrenko, and E. M. Schulson, *Philosophical Magazine B* **67**, 289 (1993).
- [13] A. K. Tagantsev, *Phys Rev B* **34**, 5883 (1986).
- [14] P. Zubko, G. Catalan, and A. K. Tagantsev, *Annu Rev Mater Sci* **43**, 387 (2013).
- [15] H. Lu, C. W. Bark, D. Esque de los Ojos, J. Alcala, C. B. Eom, G. Catalan, and A. Gruverman, *Science* **336**, 59 (2012).
- [16] J. Narvaez, F. Vasquez-Sancho, and G. Catalan, *Nature* **538**, 219 (2016).
- [17] M. M. Yang, D. J. Kim, and M. Alexe, *Science* **360**, 904 (2018).
- [18] F. Vasquez-Sancho, A. Abdollahi, D. Damjanovic, and G. Catalan, *Adv Mater* **30**, 1705316 (2018).
- [19] L. Shu *et al.*, *Nat Mater* **19**, 605 (2020).
- [20] M. Torbati, K. Mozaffari, L. Liu, and P. Sharma, *Rev Mod Phys* **94**, 025003 (2022).
- [21] See Supplemental Material for additional measurements, analysis, and details of calculations.
- [22] M. Faraday, *Journal of the Franklin Institute, of the State of Pennsylvania, for the Promotion of the Mechanic Arts; Devoted to Mechanical and Physical Science, Civil*

- Engineering, the Arts and Manufactures, and the Recording of American and Other Patent Inventions (1828-1851) **20**, 283 (1850).
- [23]N. H. Fletcher, *Philosophical Magazine* **7**, 255 (1962).
- [24]J. G. Dash, A. W. Rempel, and J. S. Wettlaufer, *Reviews of Modern Physics* **78**, 695 (2006).
- [25]B. Slater and A. Michaelides, *Nature Reviews Chemistry* **3**, 172 (2019).
- [26]I. Golecki and C. Jaccard, *Journal of Physics C: Solid state physics* **11**, 4229 (1978).
- [27]H. Dosch, A. Lied, and J. Bilgram, *Surface science* **327**, 145 (1995).
- [28]A. Döppenschmidt and H.-J. Butt, *Langmuir* **16**, 6709 (2000).
- [29]H. Bluhm, D. F. Ogletree, C. S. Fadley, Z. Hussain, and M. Salmeron, *Journal of Physics: Condensed Matter* **14**, L227 (2002).
- [30]V. Sadtchenko and G. E. Ewing, *Canadian journal of physics* **81**, 333 (2003).
- [31]M. Goertz, X.-Y. Zhu, and J. Houston, *Langmuir* **25**, 6905 (2009).
- [32]I. d. A. Ribeiro and M. d. Koning, *The Journal of Physical Chemistry C* **125**, 627 (2021).
- [33]Q. Ma, X. Wen, L. Lv, Q. Deng, and S. Shen, *Applied Physics Letters* **123** (2023).
- [34]P. Zubko, G. Catalan, A. Buckley, P. R. Welche, and J. F. Scott, *Phys Rev Lett* **99**, 167601 (2007).
- [35]P. Vales-Castro, K. Roleder, L. Zhao, J.-F. Li, D. Kajewski, and G. Catalan, *Appl Phys Lett* **113** (2018).
- [36]W. Ma and L. E. Cross, *Appl Phys Lett* **88**, 232902 (2006).
- [37]J. Narvaez and G. Catalan, *Appl Phys Lett* **104** (2014).
- [38]O. Mishima, L. Calvert, and E. Whalley, *Nature* **310**, 393 (1984).
- [39]A. K. Garg, *Physica Status Solidi (a)* **110**, 467 (1988).
- [40]X. C. Su, L. Lianos, Y. R. Shen, and G. A. Somorjai, *Phys Rev Lett* **80**, 1533 (1998).
- [41]T. Sugimoto, N. Aiga, Y. Otsuki, K. Watanabe, and Y. Matsumoto, *Nature Physics* **12**, 1063 (2016).
- [42]N. Aiga, T. Sugimoto, Y. Otsuki, K. Watanabe, and Y. Matsumoto, *Physical Review B* **97**, 075410 (2018).
- [43]S. Shen and S. Hu, *J Mech Phys Solids* **58**, 665 (2010).
- [44]A. K. Tagantsev and A. S. Yurkov, *J Appl Phys* **112**, 044103 (2012).
- [45]M. Stengel, *Phys Rev B* **90**, 201112(R) (2014).
- [46]J. Narvaez, S. Saremi, J. Hong, M. Stengel, and G. Catalan, *Phys Rev Lett* **115**, 037601 (2015).
- [47]X. Martí, P. Ferrer, J. Herrero-Albillos, J. Narvaez, V. Holy, N. Barrett, M. Alexe, and G. Catalan, *Phys Rev Lett* **106**, 236101 (2011).
- [48]X. Zhang, Q. Pan, D. Tian, W. Zhou, P. Chen, H. Zhang, and B. Chu, *Phys Rev Lett* **121**, 057602 (2018).
- [49]D. Pan, L.-M. Liu, G. A. Tribello, B. Slater, A. Michaelides, and E. Wang, *Phys Rev Lett* **101**, 155703 (2008).
- [50]H. B. Michaelson, *J Appl Phys* **48**, 4729 (1977).
- [51]O. Buser and A. Aufdermaur, in *Electrical processes in atmospheres* (Springer, 1976), pp. 294.
- [52]E. Mazzega, U. del Pennino, A. Loria, and S. Mantovani, *The Journal of Chemical Physics* **64**, 1028 (1976).

- [53]J. F. Scott, *Journal of Physics: Condensed Matter* **20** (2008).
- [54]L. S. Pedroza, A. Poissier, and M. V. Fernandez-Serra, *J Chem Phys* **142**, 034706 (2015).
- [55]T. Sugimoto and Y. Matsumoto, *Phys Chem Chem Phys* **22**, 16453 (2020).
- [56]A. Poissier, S. Ganeshan, and M. Fernandez-Serra, *Physical Chemistry Chemical Physics* **13**, 3375 (2011).
- [57]T. Takahashi, *Journal of Atmospheric Sciences* **35**, 1536 (1978).
- [58]D. J. Lacks and T. Shinbrot, *Nature Reviews Chemistry* **3**, 465 (2019).
- [59]J. Latham and B. J. Mason, *Proceedings of the Royal Society of London. Series A. Mathematical and Physical Sciences* **260**, 523 (1961).
- [60]B. J. Mason, *Proceedings of the Royal Society of London. A. Mathematical and Physical Sciences* **415**, 303 (1988).
- [61]T. Pätz, H. J. Herrmann, and T. Shinbrot, *Nature Physics* **6**, 364 (2010).
- [62]Y. Zhang, T. Pätz, Y. Liu, X. Wang, R. Zhang, Y. Shen, R. Ji, and B. Cai, *Physical Review X* **5**, 011002 (2015).
- [63]B. Baker, M. Baker, E. Jayaratne, J. Latham, and C. Saunders, *Quarterly Journal of the Royal Meteorological Society* **113**, 1193 (1987).
- [64]C. Emersic and C. Saunders, *Atmospheric Research* **98**, 327 (2010).
- [65]W. Gaskell and A. Illingworth, *Quarterly Journal of the Royal Meteorological Society* **106**, 841 (1980).
- [66]E. Jayaratne, C. Saunders, and J. Hallett, *Quarterly Journal of the Royal Meteorological Society* **109**, 609 (1983).
- [67]W. Keith and C. Saunders, *Meteorology and Atmospheric Physics* **41**, 55 (1989).
- [68]G. Caranti, E. Avila, and M. Ré, *Journal of Geophysical Research: Atmospheres* **96**, 15365 (1991).
- [69]E. E. Avila and G. M. Caranti, *Journal of Geophysical Research: Atmospheres* **99**, 10611 (1994).
- [70]M. Y. Luque, F. Nollas, R. G. Pereyra, R. E. Bürgesser, and E. E. Ávila, *Journal of Geophysical Research: Atmospheres* **125**, e2019JD030941 (2020).
- [71]R. G. Pereyra and E. E. Avila, *Journal of Geophysical Research: Atmospheres* **107**, AAC 23 (2002).
- [72]W. Gaskell, *Field and laboratory studies of precipitation charges* (The University of Manchester (United Kingdom), 1979).
- [73]P. Shaw, *Proceedings of the Royal Society of London. Series A, Containing Papers of a Mathematical and Physical Character* **94**, 16 (1917).
- [74]M. Sow, D. J. Lacks, and R. Mohan Sankaran, *J Appl Phys* **112** (2012).
- [75]L. Xie, P. He, J. Zhou, and D. Lacks, *Journal of Physics D: Applied Physics* **47**, 215501 (2014).
- [76]C. A. Mizzi, A. Y. W. Lin, and L. D. Marks, *Phys Rev Lett* **123**, 116103 (2019).
- [77]C. A. Mizzi and L. D. Marks, *Nano Lett* **22**, 3939 (2022).
- [78]S. Cho *et al.*, *Nature Communications* **15**, 387 (2024).
- [79]A. N. Aufdermaur and D. Johnson, *Quarterly Journal of the Royal Meteorological Society* **98**, 369 (1972).
- [80]W. Gaskell, *Quarterly Journal of the Royal Meteorological Society* **107**, 955 (1981).
- [81]H. Dosch, A. Lied, and J. H. Bilgram, *Surface science* **366**, 43 (1996).

- [82] V. F. Petrenko, *The Journal of Physical Chemistry B* **101**, 6276 (1997).
- [83] G.-J. Kroes, *Surface Science* **275**, 365 (1992).
- [84] W. R. Harper, (No Title) (1967).
- [85] L. S. McCarty and G. M. Whitesides, *Angewandte Chemie International Edition* **47**, 2188 (2008).
- [86] H. Zhang, S. Sundaresan, and M. A. Webb, *Nature Communications* **15**, 2616 (2024).
- [87] F. Rawlins, *Quarterly Journal of the Royal Meteorological Society* **108**, 779 (1982).
- [88] P. Ordejón, E. Artacho, and J. M. Soler, *Physical review B* **53**, R10441 (1996).
- [89] J. M. Soler, E. Artacho, J. D. Gale, A. García, J. Junquera, P. Ordejón, and D. Sánchez-Portal, *Journal of Physics: Condensed Matter* **14**, 2745 (2002).
- [90] J. P. Perdew, K. Burke, and M. Ernzerhof, *Phys Rev Lett* **77**, 3865 (1996).
- [91] M. Dion, H. Rydberg, E. Schröder, D. C. Langreth, and B. I. Lundqvist, *Phys Rev Lett* **92**, 246401 (2004).
- [92] J. Wang, G. Román-Pérez, J. M. Soler, E. Artacho, and M.-V. Fernández-Serra, *The Journal of chemical physics* **134** (2011).
- [93] B. Pamuk, J. M. Soler, R. Ramírez, C. P. Herrero, P. W. Stephens, P. B. Allen, and M.-V. Fernández-Serra, *Phys Rev Lett* **108**, 193003 (2012).
- [94] B. Pamuk, P. B. Allen, and M. V. Fernández-Serra, *Physical Review B* **92**, 134105 (2015).
- [95] J. A. Morrone and R. Car, *Phys Rev Lett* **101**, 017801 (2008).

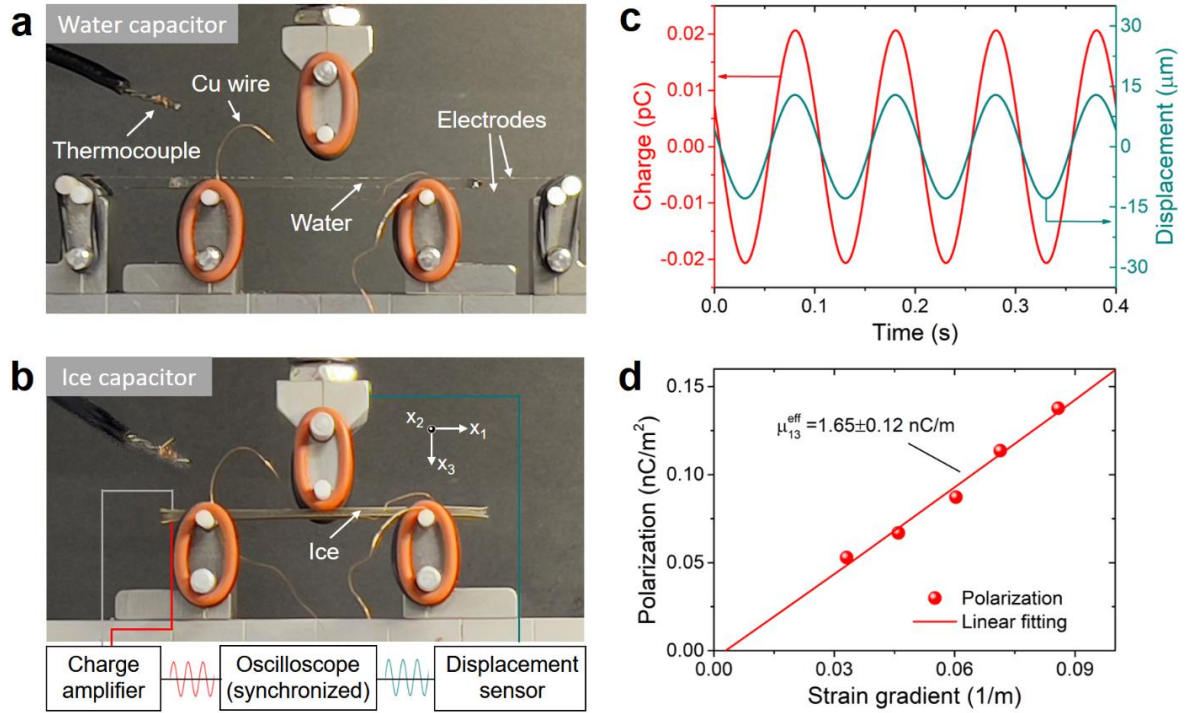


**Fig. 1 Experimental setup for measuring ice flexoelectricity.** **a**, A water capacitor, consisting of a layer of water and two pieces of Au electrodes. **b**, An ice capacitor placed in the DMA for oscillating three-point bending deformation. The displacement in the center and the bending-induced electric charge are recorded by an oscilloscope synchronously. **c**, Fourier-filtered first-harmonic displacement (the cyan curve) and charge (the red curve) for an applied displacement of  $12.5 \mu\text{m}$ . **d**, Electric polarization versus strain gradients, and linear fit to the results. The data in (c) and (d) was obtained at 237 K.

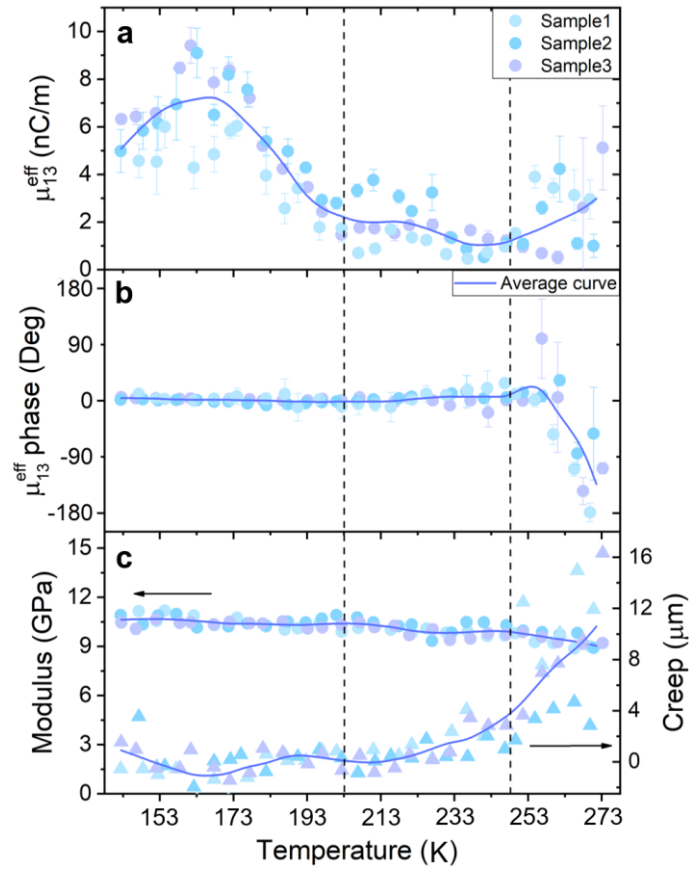


**Fig. 2. Temperature dependence of ice flexoelectricity and mechanical properties.** **a**, The effective flexoelectric coefficient as a function of temperature. **b**, The phase angle between displacement and polarization charge as a function of temperature. **c**, The modulus and the creep displacement in the first ten seconds of loading as a function of temperature. The data shown in this figure is obtained in three samples with Au electrodes. The solid lines represent the smoothed average curve. The error bars in (a) and (b) represents the standard error from linear regressions and averages respectively.



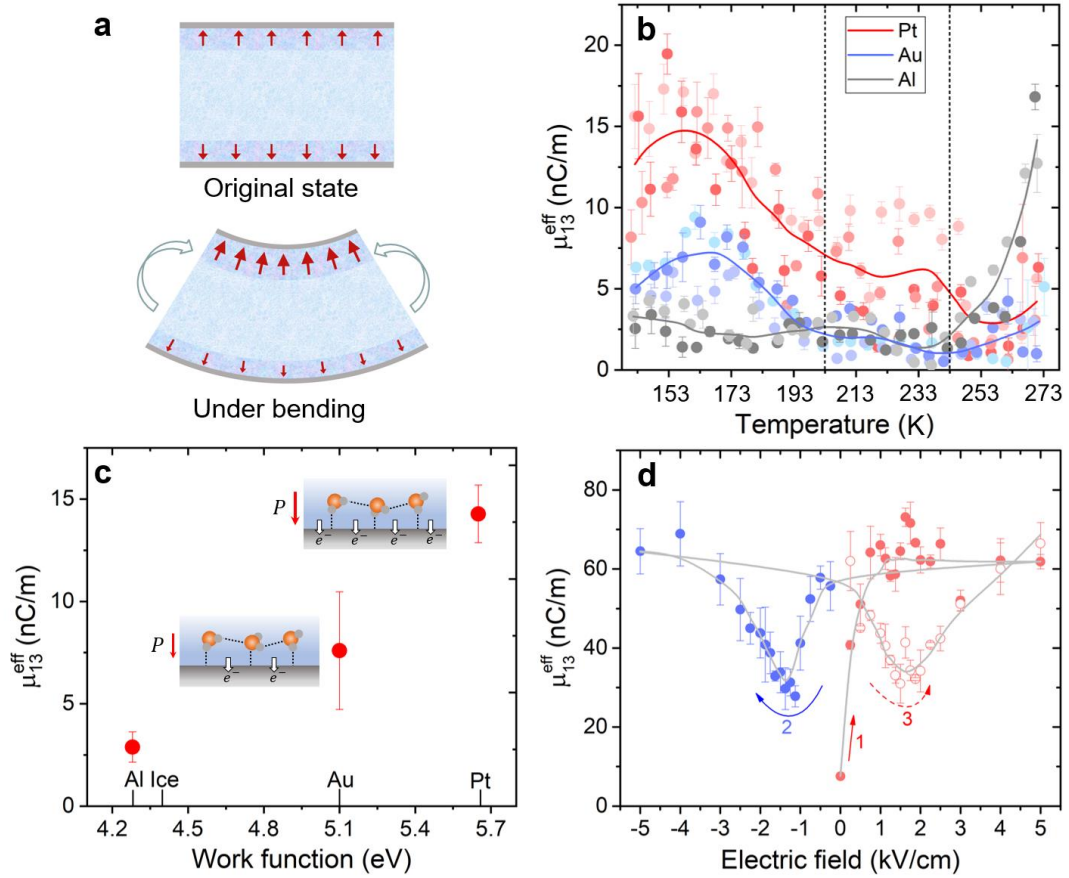


**Fig. 3. Surface contribution to enhanced flexoelectricity.** **a**, Schematic illustration of how surface polarization can contribute to effective flexoelectricity in a slab with polar surface layers. **b**, Experimental flexoelectric coefficient of ice with Pt, Au, and Al electrodes as a function of temperature. The solid lines are a smooth average of all the capacitors having the same type of electrode. The electrode-dependent results indicate a dependence of flexoelectricity on surface boundary condition. **c**, Value of the flexoelectricity at 163 K as a function of the electrode work functions. **d**, The evolution of flexoelectricity as a function of poling electric field measured at  $\sim 155$  K and with Au electrodes. The error bars in (b) represent the standard error from linear regressions. The error bars in (c) and (d) represent the standard error from averages of (c) different samples or (d) multiple measurements.

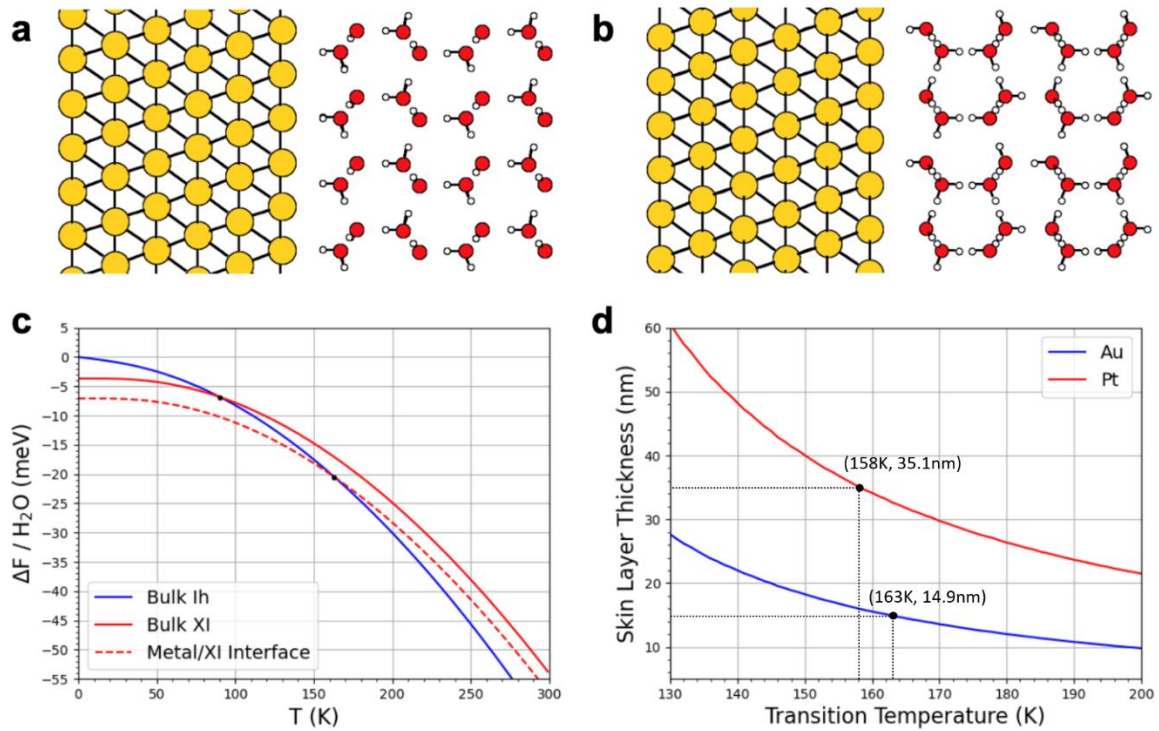


**Fig. 4.** *Ab initio* simulations of metal [111]-ice (Ih and XI) [001] interfaces. **a**, Illustration of the Ice XI / Au[111] system. **b**, Illustration of the Ice Ih / Au[111] system. **c**, Relative free energy for ice XI and ice Ih, showing that the transition temperature  $T_c$  is increased within the metal/ice interface than that in the bulk ice[94]. **d**, Relationship between the increased  $T_c$  and the skin layer thickness for Au[111] and Pt[111].

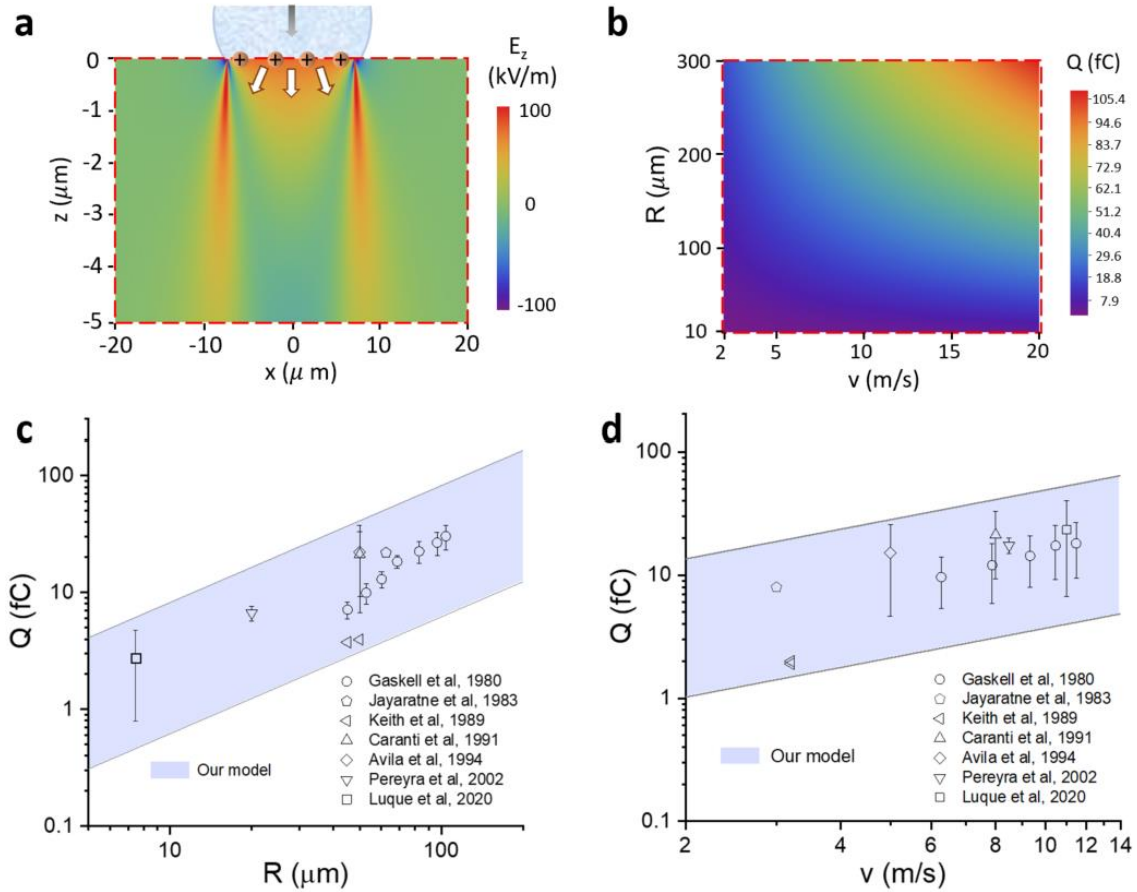


**Fig. 5. Flexoelectricity in ice electrification events.** **a**, Calculated distribution of the vertical flexoelectric field beneath the indentation surface. **b**, Calculated dependence of the flexoelectric bound charge  $Q$  on particle radius  $R$  and velocity  $v$ . This bound charge is expected to be neutralized by transferring free charges in the quasi-liquid layers across the contact interface. **c**,  $Q$  versus  $R$  when  $v=8\text{ m/s}$ . **d**,  $Q$  versus  $v$  when  $R=50\text{ }\mu\text{m}$ . **c** and **d** show quantitative agreements between our calculations and the transferred charge reported in previous experiments[65-72]. Similar comparisons of  $Q$  versus effective force and kinetic energy can be found in Fig. S12c and d in Supplemental Material[21].

# Supplementary Information for

## Flexoelectricity and surface ferroelectricity of water ice

**Authors:** X. Wen<sup>1,3</sup>, Q. Ma<sup>1</sup>, A. Mannino<sup>4,5</sup>, M. Fernandez-Serra<sup>4,5</sup>, S. Shen<sup>1\*</sup>, G. Catalan<sup>2,3\*</sup>

**Affiliations:**

<sup>1</sup>State Key Laboratory for Strength and Vibration of Mechanical Structures, School of Aerospace Engineering, Xi'an Jiaotong University, Xi'an, China.

<sup>2</sup>ICREA—Institutio Catalana de Recerca i Estudis Avançats, Passeig Lluís Companys 23, Barcelona, Catalonia

<sup>3</sup>Institut Catala de Nanociencia i Nanotecnologia (ICN2), CSIC and The Barcelona Institute of Nanoscience and Technology (BIST), Campus Universitat Autònoma de Barcelona, Bellaterra, Catalonia.

<sup>4</sup>Physics and Astronomy Department, Stony Brook University, Stony Brook, New York 11794-3800, United States

<sup>5</sup>Institute for Advanced Computational Science, Stony Brook University, Stony Brook, New York 11794-3800, United States

\*Corresponding author. Email: sshen@mail.xjtu.edu.cn; gustau.catalan@icn2.cat

### **S1. Excluding bending-induced phase transition**

Pressure-induced phase transition in ice is a well-known effect, but it can be excluded in our experiments, because the actual stress at the surface is too small compared to the energies involved in structural phase transitions of ice. To illustrate this, we have performed a finite element simulation (COMSOL Multiphysics 5.3) using the same geometric parameters, material properties, and mechanical boundary conditions of our experiments. Fig. S6 shows the distribution of the in-plan stress  $\sigma_{11}$  across the beam under the maximum force (2.5N) used in our experiments. As expected, the beam experiences compression on one side and stretching on the other side; and the maximum bending-induced stress at the surface is  $\sim 0.005$  GPa. This is orders-of-magnitude smaller than the pressure needed to induce a phase transition to ice IX ( $\sim 0.2$  GPa[1,2]) or amorphization ( $\sim 1$  GPa[3]).

### **S2. Analysis of the contribution from grain boundaries**

While indeed our samples are polycrystalline and grain boundaries are non-centrosymmetric, the grain-boundary contribution to the total flexoelectric effect can be neglected, both on theoretical and on experimental grounds. Theoretically, we must remember that at each grain boundary there are two opposing surfaces, corresponding to the adjacent grains. These surfaces have opposite orientation and, therefore, on average their surface-piezoelectric contributions must cancel each other. As indirect evidence, the flexoelectricity of BaTiO<sub>3</sub> and SrTiO<sub>3</sub> has been studied in ceramics[4,5] and single crystals[6,7], finding no significant difference of flexoelectric coefficient, suggesting that the existence of grain boundaries in ceramics does not significantly affect the flexoelectric outcome. To provide direct experimental evidence for lack of grain boundary contributions, we have performed new flexoelectric experiments with different grain sizes, achieved by annealing the sample for different durations at 267 K, during which ice grains recrystallized and changed grain sizes (Fig. S7a~c). All flexoelectric measurements fell into the range of 1~3 nC/m (Fig. S7d) as we summarized in the manuscript, and no conclusive effect of grain size on ice flexoelectricity was observed.

### **S3. Ab initio calculation of the piezoelectric constant of ice XI**

The unit cell for this calculation is an ice XI unit cell with 4 water molecules. The exchange-correlation functional is VDW/DRSLL. The lattice vectors have the following form:  $[0, a, 0]$ ,  $[a\sqrt{3}/2, a/2, 0]$ ,  $[0, 0, c]$  with lattice parameters  $a$  and  $c$ . First, we adjust  $c$  with a fixed lattice constant,  $a$ , and run a SIESTA calculation that allows the “out-of-plane” H atoms to relax. We then determine the most energetically favorable configuration and repeat this for several values of  $a$  (Fig. S9a). Mulliken charges for each atom in the system are computed by SIESTA[8,9], and we use them to calculate the polarization in the  $c$ -direction. Finally, we plot the polarization as a function of the strain on the lattice constant (Fig. S9b). The slope of this plot is the transverse piezoelectric constant  $e_{13}$ , which was found to be  $0.32$  C/m<sup>2</sup>.

### **S4. Surface piezoelectricity**

Fig. 3a schematically shows how surface ferroelectricity can contribute to effective flexoelectricity. In a dielectric sample with polar skin layers at the surface, the surface-piezoelectric contribution to the total effective flexoelectricity is[10,11]

$$\mu_{13}^{eff} = e_{13}^{surf} \lambda \frac{h\varepsilon_b}{2\lambda\varepsilon_b + h\varepsilon_\lambda} \quad (S1)$$

where  $e_{13}^{surf}$  is the transverse surface piezoelectric constant,  $\lambda$  and  $h$  are the thickness of the skin layer and the bulk,  $\varepsilon_\lambda$  and  $\varepsilon_b$  are the dielectric constant of the skin layer and the bulk respectively. When  $\lambda$  is much thinner than  $h$  ( $\frac{\lambda}{h} \ll 1$ ), equation (S1) can be simplified as

$$\mu_{13}^{eff} = e_{13}^{surf} \lambda \frac{\varepsilon_b}{\varepsilon_\lambda} \quad (S2)$$

By subtracting the bulk contribution ( $\sim 2$  nC/m) from the measured flexoelectric peak ( $\sim 7.6$  nC/m), we can obtain a surface-contributed  $\mu_{13}^{eff}$  of  $\sim 5.6$  nC/m in Au-electrodes samples.  $e_{13}^{surf} = 0.32$  C/m<sup>2</sup> is obtained in Section 3 by ab initio calculations. We assume that the dielectric constant of the skin layer is similar to that of the bulk, i.e.,  $\varepsilon_b/\varepsilon_\lambda = 1$ . Substituting these parameters in equation (S2), we estimate the skin-layer thickness  $\lambda$  at Au/ice interface to be  $\sim 17.5$  nm. The surface-contributed  $\mu_{13}^{eff}$  in Pt-electrodes samples is  $\sim 10$  nC/m, leading to a skin layer thickness  $\lambda$  at Pt/ice interface of  $\sim 31.3$  nm.

According to equation (S2), the effective flexoelectric coefficient only depends on the thickness of the skin layer  $\lambda$ , and is independent from the bulk sample thickness  $h$ . As demonstrated in previous works[12,13], the flexoelectric coefficient can only be proportional to sample thickness when the samples are semiconductors with Schottky junctions, which is not the case for ice. The independence on bulk thickness may seem counter-intuitive for a claimed surface property, but it is in fact reasonable. When a beam is bent with a given curvature, increasing sample thickness linearly reduces the surface/volume ratio but, at the same time, linearly increases the surface strain. The two opposite dependencies mutually cancel, resulting in no bulk thickness dependence. This conclusion has been affirmed in the theoretical literature[10,11] and is backed by our own flexoelectric measurements for samples with different thicknesses (from 1mm to 2mm), as shown in Fig. S10 below.

## S5. Ab initio calculation of relative energy between ice-metal interface

### A. Cohesive energy calculations at T=0.

Simulating these systems and being able to compare them is not trivial due to the polar nature of the ice XI phase. The limitations on the size of the system that can be computationally accessible poses a general problem when studying water or ice interfacial properties using ab initio simulations. In the case of ice XI, two different options to study the interface are presented in Fig. S11. These are non-ideal. In the case of (a) two different interfaces with the metal are computed in one calculation. One with the protons facing the metal and (positive end of the polarized slab) and one with the O atoms facing the metal (negative end of the slab). The polarization is screened by the metal, but it is difficult to separate the contributions from the two interfaces. It is possible to create a proton ordered slab with symmetric interfaces as in (b), both of them with the presumed favorable H-Metal interface. However, in order to do this one

needs to create a layer of H-bond defects in the middle of the slab. These are water molecules not completely satisfying Bernal–Fowler–Pauling ice rules (There is always a proton in between each pair of oxygen atoms and each oxygen always keeps two close, covalently bound protons). When comparing these structures to a proton disordered system (which always has, by definition, symmetric interfaces), the proton disordered system will always be more stable. Hence it is necessary to account for the defect formation energy, and this makes the calculation much more complicated. We can calculate the cohesive energy per water molecule with the following equation:

$$E_{\text{Cohesive}/\text{H}_2\text{O}} = E_{\text{Ice}/\text{Metal}} - E_{(\text{Ice}-\text{H}_2\text{O})/\text{Metal}} - E_{\text{H}_2\text{O}} \quad (\text{S3})$$

with the subscripts denoting which species are included in the calculation. In the second term, we remove a single water molecule from the surface layer of the ice. The unit cell and all other simulation parameters remain the same.

This calculation is done for system (b) and a similar system (c) with ice Ih. The difference in cohesive energy for these two systems is 233 meV with system (b) being more favorable. We also do this calculation for bulk ice XI and bulk ice Ih without the Au slab. The difference in cohesive energy for these two systems is 93 meV with the bulk ice XI system being more favorable. We conclude from this that the Au interface creates an enhanced stability ( $\Delta E_{\text{Surface}}$ ) of 140 meV. As the number of ice bilayers increases, we anticipate this enhanced stability will be proportional to the surface-to-volume ratio. From our previous work<sup>[14]</sup>, we have shown that the bulk limit for the relative energy per water molecule between ice XI and ice Ih is 3.68 meV. The final energy calculation at 0 K is as follows:

$$E_{\text{Relative}/\text{H}_2\text{O}}^{\text{T}=0} = \frac{\Delta E_{\text{Surface}}}{N_{\text{Bilayers}}} - 3.68 \text{ meV} \quad (\text{S4})$$

We can perform a similar analysis with a Pt slab. As shown in the previous section, we expect the skin layer thickness to be much larger with Pt electrodes, thus the stability of the proton ordered interface should be enhanced by much more than 140 meV. In this case, it is more straightforward to use the fully ferroelectric system shown in Fig.S11a to determine the difference in stability between the ice XI-Au[111] and ice XI-Pt[111] interfaces. Near the center of the ice XI slab, the Pt system is favored by 38 meV. This increases to 205 meV at the interface, implying a surface enhancement of 167 meV. Adding this to the previously discussed enhanced stability in Au of 140 meV, we find that the proton ordered (XI) interface with Pt has an enhanced stability ( $\Delta E_{\text{Surface}}$ ) of 307 meV relative to the proton disordered (Ih) interface with Pt.

### **B. Free energy differences versus Temperature.**

The treatment of nuclear quantum effects will be summarized here and is described in full detail in our previous work<sup>[14]</sup>. We define  $V_0$  to be the volume that minimizes the Born-Oppenheimer energy,  $E_0(V)$ . We can expand this energy in a Taylor series for small perturbations from  $V_0$ .

$$E_0(V) = E_0(V_0) + \frac{B_0}{2V_0} (V - V_0)^2 \quad (\text{S5})$$

The phonon frequencies can also be expanded in this way.

$$\omega_k(V) = \omega(V_0) \left(1 - \gamma_k \frac{V-V_0}{V_0}\right) \quad (\text{S6})$$

In these expansions,  $B_0$  is the dominant part of the bulk modulus with vibrational corrections removed.  $\gamma_k$  are the mode Grüneisen parameters, defined as

$$\gamma_k = -\frac{\partial(\ln\omega_k)}{\partial(\ln V)} = -\frac{V}{\omega_k} \frac{\partial\omega_k}{\partial V}. \quad (\text{S7})$$

We calculate the phonon frequencies,  $\omega_k$ , at three different volumes and calculate its volume dependence to linear order. This adds a volume dependence to the Helmholtz free energy  $F(V, T)$ [15] of independent harmonic oscillators.

$$F(V, T) = E_0(V) + \sum_k \left[ \frac{\hbar\omega_k(V)}{2} + k_B T \ln(1 - e^{-\hbar\omega_k(V)/k_B T}) \right] - TS_H \quad (\text{S8})$$

The sum is over both phonon branches and phonon wave vectors within the Brillouin zone.

The entropy of the proton disorder,  $S_H$ , is included in the last term of the free energy equation. This entropy is zero for ice XI (proton-ordered ice). Pauli has estimated that the entropy for ice Ih (proton-disordered ice) is  $Nk_B \ln(3/2)$ , which was obtained theoretically[16] and experimentally[17,18].

We can find the classical limit of the free energy by taking the high-temperature limit of (S8).

$$F(V, T) = E_0(V) + \sum_k \left( k_B T \ln \left\{ \frac{\hbar\omega_k[V(T)]}{k_B T} \right\} \right) - TS_H \quad (\text{S9})$$

In Fig 4c of the manuscript, we show the free energies of bulk ice Ih and bulk ice XI as a function of temperature. The difference between these two free energies should match the enhanced stability described in the previous section at the transition temperature.

$$\Delta F_{(XI-Ih)/H_2O}(T_C) = -\left(E_{\text{Relative}/H_2O}^{T=0} + 3.68 \text{ meV}\right) \quad (\text{S10})$$

The skin layer thickness,  $h$ , can be found from the number of bilayers with the conversion factor 0.3615 nm / 1 bilayer. After combining (S4) and (S10), we are left with the following equation:

$$h(T_C) = \frac{\Delta E_{\text{Surface}} \cdot 0.3615 \text{ nm}}{\Delta F_{(XI-Ih)/H_2O}(T_C)} \quad (\text{S11})$$

Substituting the experimentally obtained phase-transition temperatures into equation (S11), we find  $h$  to be 14.9 nm for Au and 35.1 nm for Pt, in reasonable agreement with the experimentally estimated  $h$  of 17.5nm for Au and 31.3nm for Pt in Section4.

## S6. The free charge on ice surfaces and the redistribution by flexoelectricity

The screening charge comes from mobile ions ( $H^+$ ,  $OH^-$ , and other impurities) in the interfacial quasi-liquid layers (QLL), as justified below. The existence of a QLL with thickness of 1~100 nm on the surface of ice has been verified by many techniques[19-24] and summarized by authoritative review articles[25-27]. Our own data also indicate the appearance of QLL above 248K (Fig. S4). The existence of QLL layers is thus not in doubt, but the key question is whether it contains free ionic charges. The ionic charge density in QLL has been determined to be in the range of  $10^{-3} \sim 10^{-2}$  C/m<sup>2</sup> by synchrotron X-radiation[28], scanning force microscopy[29], and molecular dynamic calculations[30]. This charge density is more than sufficient to compensate our calculated flexoelectric polarization ( $10^{-5} \sim 10^{-4}$  C/m<sup>2</sup>). In addition,



a volta-effect measurement[31] confirms that the appearance of the QLL above 243K alters the ice surface potential by  $\sim 100\text{mV}$ , which indicates the change in charge density at the surface and is indeed comparable with the zeta potential of the ice/water interface[32,33]. Hall-effect measurements additionally indicate that the mobility of surface charge carriers of ice ( $\sim 3 \times 10^{-4} \text{ m}^2/\text{Vs}$ ) is three orders of magnitude than that in water and bulk ice[34,35]. The abundant literature on the matter thus provides overwhelming evidence that ice particles are coated with a QLL that contains mobile charges capable of responding to electric fields. In the literature, it is also acknowledged that QLL ions are the most promising candidate for offering transferred charge in ice electrification problem[25,36-39].

The next question is how the charge carriers from the QLL are redistributed by flexoelectricity. To answer this question, we will base our discussion on the classic ion-transfer theory of contact electrification as first described by Henry[40], highlighted in Harper's book[41] and Lowell's review[42], and formulated in detail by Whitesides[43], who incorporated the concept of "water bridge"[44] and proposed that "*the well-known phenomenon of contact electrification may, in many circumstances, be due to the unequal partitioning of aqueous ions (particularly  $H^+$  and  $OH^-$ ) between interfaces*[43]." Whitesides' model has been supported by recent studies[45,46] and is a suitable foundation to analyze the case of ice with surface QLL ions. The potential energy landscape of ions residing on two adjacent surfaces has a double-well shape. Anything that breaks symmetry can skew the double well and thus drive the redistribution of surface ions between the two surfaces, such as the differences of ion concentration and ion affinity between two surfaces[43]. For chemically identical materials, where the above two factors are unavailable, other thermodynamic forces can also break the symmetry of energy double well and drive the charge transfer from one to another, such as temperature gradient[42,47,48] and external electric field[45,49,50]. However, ice-collision-induced charge transfer has been observed even in the absence of external electric field and temperature gradient[51-57]. In this scenario, flexoelectricity emerges as an effect that is (i) universal, and (ii) able to create an electric field that can skew the double well of potential energy landscape for surface ions, and therefore drive ion redistribution between two surfaces (Fig. S12b). The capability of flexoelectricity to skew thermodynamic double-wells is well known and has been demonstrated in ferroelectrics[58,59].

## **S7. Discussion of some explanations for CE and the applicability to ice**

- 1) Piezoelectricity. Ice-Ih is not piezoelectric, which is well-known[60] and also confirmed by our experiments (Fig. S2). Therefore, this proposal can be excluded.
- 2) Work function difference. This is the classic mechanism for the CE of metals and semiconductors[41,61], but it cannot explain the CE between chemically identical materials. Although size may modify work function in the same material, this effect is negligible for particles with a radius above 1 micron[62,63], so we can exclude it too.
- 3) Workman-Reynolds freezing potential. The process of freezing dilute aqueous solutions can lead to charge separation due to unequal incorporation of solute ions into ice lattice, suggested to contribute to the CE between ice particles and supercooled water droplets[64,65].

Such freezing potential, however, is found to develop very slowly and cannot explain the significant CE with short contact time in thunderstorms[66-68].

4) External electric field. Although the presence of an external electric field facilitates the CE between chemically identical insulators[45,49,50,69], there is plenty of evidence showing that the CE of ice can also occur in the absence of such a field[51-57,70,71]. Moreover, it seems like a circular justification considering that the built-up electric field (the cause of lightning) is known to be the consequence of the CE of ice particles[25,66,72,73], rather than its cause. Also, invoking external electric field requires answering the question of where they come from. The electric field argument can in fact be coopted in support of our model just by noticing that flexoelectricity generates electric fields.

5) Temperature difference. The thermoelectric effect has been used to explain the CE of ice (and other insulators) under a temperature difference  $\Delta T$  between two contact bodies[47,74,75], which is assumed to be either pre-existing or generated by unequal friction heat (so-called asymmetric contact[41,48,63]). However, many studies have reported results that contradict this explanation, including the observed CE of ice in the absence of  $\Delta T$  or the observed CE in the presence of  $\Delta T$  but with a charge-transfer direction opposite to the theoretical prediction[51,52,57,70]. Therefore, it has been accepted that this proposal is not the main mechanism responsible for the CE of ice[25,66].

6) Surface ion concentration difference. This is the most popular explanation so far for the CE of ice[25,66,76]. It suggests that if ice and graupel particles are both grown from vapor and with different growth rates, the two surfaces would process different charge densities in the QLL that drives ion diffusion (transfer) during contact[25,66,76-80]. However, the CE of ice has also been observed when both ice and graupel were grown from freezing droplets instead of vapor[38,51,55,57,70]. In line with this, this explanation has clear shortcomings, and C.P.R. Saunders, one of its inventors[77], commented[76] *“it offers no ability to quantitatively predict the magnitude of charge transferred during ice particle collisions, nor insight into explicit physical, microscopic charge transfer processes”* and restated[80] in 2020 *“This is a qualitative empiricism and is, by definition, not capable of providing quantitative predictions”*.

7) Mechanochemistry/fractures/mass transfer. It is not surprising that the contact between two surfaces can involve the breaking of chemical bonds, exposure of new surfaces, and mass transfer. This has stimulated the field to study the connection between mechanochemistry and the CE for insulators (including ice)[74,78,81-84]. However, it is challenging to quantitatively evaluate the role of mechanochemistry in the CE, given the enormous uncertainties involved. Additionally, this explanation still needs to incorporate a thermodynamic force to explain the charge transfer between chemically identical insulators. In this context, it is worth mentioning that the flexoelectricity around defects (i.e., dislocations, fractures) is significant[85-88], and in suitable environments, strain gradients can facilitate chemical reactions (aka flexo-catalysis)[89-92]. Moreover, there is experimental evidence that frictional wear of surfaces depends on flexoelectricity[93]. Tribological mass transfer should therefore not be seen as a separate mechanism from flexoelectricity.

The common message of these excellent studies is that the understanding of the CE of ice is complex and far from complete. It can involve different physical mechanisms that can co-exist and interact in subtle ways, which may explain why it remains unsolved till now as one of the earliest scientific problems of all time. As C.P.R. Saunders, an expert working on the CE of ice[52,66,77], commented recently[80] that “*meaningful forecasts of storm electrical evolution and lightning properties are not currently possible because there remains poor understanding of the fundamental physics of the underlying mechanisms that account for cloud charging and the complex charge distributions observed.*” Rohan Jayaratne, another expert in the field[52,77], also pointed out that recently[94] that “*these various hypotheses have been found to be inconsistent with the experimental evidence when subjected to careful scrutiny, and a new direction of approach to understanding the microphysical charging mechanism is necessary*”. It is not our intention to claim ice flexoelectricity as *the* new direction of approach that will put an end to such a long-standing debate, but to show that its contribution to the CE of ice cannot be ignored, since it is conceptually inevitable (flexoelectricity is generated in any inhomogeneous deformation), and quantitatively important.

### S8. Calculation of flexoelectric polarization and field

Flexoelectric polarization is defined as[95,96]

$$P_i = \mu_{ijkl} \frac{\partial \varepsilon_{kl}}{\partial x_j} \quad (S12)$$

where  $\mu_{ijkl}$  is the fourth-rank tensor of flexoelectric coefficients,  $P_i$  is the electric polarization,  $\varepsilon_{kl}$  is the strain tensor, and  $x_j$  is the position coordinate. We consider three components of  $\mu_{ijkl}$  (longitudinal  $\mu_{1111}$ , transversal  $\mu_{1122}$ , and shear  $\mu_{1212}$ ) in our calculations, which can be rewritten in the Voigt notation as  $\mu_{11}$ ,  $\mu_{12}$ , and  $\mu_{44}$ , respectively. The polarization field in Cartesian coordinates can be written as[97,98]

$$\begin{aligned} P_x &= \mu_{11} \frac{\partial \varepsilon_{xx}}{\partial x} + \mu_{12} \left( \frac{\partial \varepsilon_{yy}}{\partial x} + \frac{\partial \varepsilon_{zz}}{\partial x} \right) + 2\mu_{44} \left( \frac{\partial \varepsilon_{xy}}{\partial y} + \frac{\partial \varepsilon_{xz}}{\partial z} \right) \\ P_y &= \mu_{11} \frac{\partial \varepsilon_{yy}}{\partial y} + \mu_{12} \left( \frac{\partial \varepsilon_{xx}}{\partial y} + \frac{\partial \varepsilon_{zz}}{\partial y} \right) + 2\mu_{44} \left( \frac{\partial \varepsilon_{xy}}{\partial x} + \frac{\partial \varepsilon_{yz}}{\partial z} \right) \\ P_z &= \mu_{11} \frac{\partial \varepsilon_{zz}}{\partial z} + \mu_{12} \left( \frac{\partial \varepsilon_{xx}}{\partial z} + \frac{\partial \varepsilon_{yy}}{\partial z} \right) + 2\mu_{44} \left( \frac{\partial \varepsilon_{xz}}{\partial x} + \frac{\partial \varepsilon_{yz}}{\partial y} \right) \end{aligned} \quad (S13)$$

Since it is not possible to measure separately each of the tensor components, we set  $\mu_{11}$ ,  $\mu_{12}$ , and  $\mu_{44}$  equal to the measured  $\mu^{eff}$  and obtain the flexoelectric polarization from equation (S13) using the calculated strain gradients (see the next section). Flexoelectricity can also act as an effective electric field[58]. The flexoelectric field in isotropic solids (relative permittivity  $\xi_r$  is a constant) is given by[95,96]

$$E_x = \frac{P_x}{\xi_0(\xi_r - 1)}, \quad E_y = \frac{P_y}{\xi_0(\xi_r - 1)}, \quad E_z = \frac{P_z}{\xi_0(\xi_r - 1)} \quad (S14)$$

### S9. Calculation of flexoelectricity in the contact region of ice collisions.

The classical Hertzian theory of contact mechanics[99] has been widely used to estimate the strain distributions and the associated flexoelectricity in contact problems[100-102]. Since the size of ice particles ( $R_1$ ) is often orders of magnitude larger than that ( $R_2$ ) of graupel

particles[60,66] and the modulus of the former ( $Y_1$ ) is larger than that of the latter ( $Y_2$ ), we treat the ice particle as an indenter with radius of  $R$  and treat the graupel particle as a semi-infinite elastic space. Then we can adopt Hertzian theory to calculate the strain distributions in graupel particles under the indentation of the small ice particle. To do so, we need to convert the impact of the indenter on the semi-space to an effective force  $F_{eff}$  by[103]

$$F_{eff} = \frac{4}{3} Y_{eff} \sqrt{R} \left( \frac{15mv_r^2}{16Y_{eff}\sqrt{R}} \right)^{3/5} \quad (S15)$$

where  $Y_{eff}$  is the effective Young's modulus of the contact,  $v_r$  is the relative velocity of the indenter moving toward the self-half space,  $m$  is the mass of the indenter which is equal to  $\frac{4}{3}\rho\pi R^3$  ( $\rho$  refers to the mass density).  $Y_{eff}$  is given by[99]

$$\frac{1}{Y_{eff}} = \frac{1-\nu_1^2}{Y_1} + \frac{1-\nu_2^2}{Y_2} \quad (S16)$$

where  $Y_1$ ,  $Y_2$  and  $\nu_1$ ,  $\nu_2$  are the Young's modulus and Poisson's ratio of the indenter and the semi-space, respectively. Under load  $F_{eff}$ , the contact radius  $a$  and mean pressure  $P_m$  on the contact surface can be expressed as[99]

$$a = \sqrt[3]{\frac{3F_{eff}R}{4Y_{eff}}}, \quad P_m = \frac{F_{eff}}{\pi a^2} \quad (S17)$$

The stress fields of the semi-space beneath the contact region of a spherical indenter in cylindrical coordinates are given by[99]

$$\sigma_{rr} = \frac{3p_m}{2} \left\{ \frac{1-2\nu}{3} \frac{a^2}{r^2} \left[ 1 - \left( \frac{z}{\sqrt{u}} \right)^3 \right] + \left( \frac{z}{\sqrt{u}} \right)^3 \frac{a^2 u}{u^2 + a^2 z^2} + \frac{z}{\sqrt{u}} \left[ u \frac{1-\nu}{a^2 + u} + (1+\nu) \frac{\sqrt{u}}{a} \tan^{-1} \frac{a}{\sqrt{u}} - 2 \right] \right\} \quad (S18)$$

$$\sigma_{\theta\theta} = -\frac{3p_m}{2} \left\{ \frac{1-2\nu}{3} \frac{a^2}{r^2} \left[ 1 - \left( \frac{z}{\sqrt{u}} \right)^3 \right] + \frac{z}{\sqrt{u}} \left( 2\nu + u \frac{1-\nu}{a^2 + u} - (1+\nu) \frac{\sqrt{u}}{a} \tan^{-1} \frac{a}{\sqrt{u}} \right) \right\} \quad (S19)$$

$$\sigma_{zz} = -\frac{3p_m}{2} \left\{ \left( \frac{z}{\sqrt{u}} \right)^3 \frac{a^2 u}{u^2 + a^2 z^2} \right\} \quad (S20)$$

$$\sigma_{rz} = -\frac{3p_m}{2} \left( \frac{rz^2}{u^2 + a^2 z^2} \right) \left( \frac{a^2 \sqrt{u}}{a^2 + u} \right) \quad (S21)$$

where  $u$  is the displacement of points on the contact surface, and can be expressed as

$$u = \frac{1}{2} \left[ (r^2 + z^2 - a^2) + \sqrt{(r^2 + z^2 - a^2)^2 + 4a^2 z^2} \right] \quad (S22)$$

The strain beneath the contact region in cylindrical coordinates can be expressed by the isotropic Hooke's law

$$\begin{aligned} \varepsilon_{rr} &= \frac{1}{Y} [\sigma_{rr} - \nu(\sigma_{\theta\theta} + \sigma_{zz})] \\ \varepsilon_{\theta\theta} &= \frac{1}{Y} [\sigma_{yy} - \nu(\sigma_{rr} + \sigma_{zz})] \\ \varepsilon_{zz} &= \frac{1}{Y} [\sigma_{zz} - \nu(\sigma_{rr} + \sigma_{\theta\theta})] \\ \varepsilon_{rz} &= \frac{1+\nu}{Y} \sigma_{rz} \end{aligned} \quad (S23)$$

According to equation (S13) and the axial symmetry in this problem, the vertical polarization  $P_z$  beneath the contact region can be written in cylindrical coordinates as

$$P_z = \mu_{11} \frac{\partial \varepsilon_{zz}}{\partial z} + \mu_{12} \left( \frac{\partial \varepsilon_{rr}}{\partial z} + \frac{\partial \varepsilon_{\theta\theta}}{\partial z} \right) + 2\mu_{44} \frac{\partial \varepsilon_{rz}}{\partial r} \quad (S24)$$

Combining equations (S15) to (S24) and adopting typical parameters in an ice-collision event (Table S1), we have computed the distributions of the flexoelectric polarization beneath the indentation surface analytically. Fig. 5a shows the vertical flexoelectric field in a specific case with  $Y_2=5$  GPa,  $\mu=5$  nC/m,  $v=8$  m/s,  $R=50$   $\mu$ m, with the corresponding flexoelectric polarization (using equation (S14)) shown in Fig. S12a. Integrating  $P_z$  over the contact area, we have further calculated the flexoelectric surface charge  $Q$ , and its dependences on particle radius and velocity. Fig. 5b shows the specific case of varying radius and velocity with  $Y_2=5$  GPa and  $\mu=5$  nC/m.

Despite numerous papers about ice-collision-induced charge separation, it is not easy to directly compare theoretical model and experiments, as the latter were usually reported under different experimental conditions that were not always fully described and/or where more than one experimental parameter was changed. In our manuscript, we selected seven experimental papers[51-57], published from 1980 to 2020, to compare with our theory controlling for each variable separately. Gaskell's classic work[51,104], which had the best-described experimental conditions, was selected as a benchmark for comparison with the following parameters:  $R=50$   $\mu$ m,  $v=8$  m/s,  $T=263$  K. To investigate the effect of particle size  $R$  on the contact-electrification charge  $Q$  (Fig. 5c), we use our model to extrapolate experiments with different velocities (at  $\sim 263$  K) to obtain a normalized  $Q$  at the reference velocity  $v=8$  m/s for comparison. Similarly, to calculate the dependence of  $Q$  on velocity (Fig. 5d), we extrapolated these experiments (at  $\sim 263$  K) with different particle size  $R$  to obtain a standardized  $Q$  at the reference radius  $R=50$   $\mu$ m for comparison. Note that these papers used diameter as particle size, but here we convert them to radius unit. The upper limit and lower limit in Fig. 5c,d comes from the selection ranges of  $\mu$  and  $Y_2$  in Table S1. The calculated results quantitatively reproduce the dependence of charge on particle size and velocity reported in previous experiments[51-57]. Using equation (S15), we can also plot the dependence of  $Q$  on the effective force (Fig. S12c). By plotting  $Q$  as a function of kinetic energy  $\frac{1}{2}mv^2$  (Fig. S12d), which simultaneously incorporates both dependencies on  $R$  and  $v$ , we can compare our model and raw experimental data without extrapolation, which shows the quantitative consistence again.

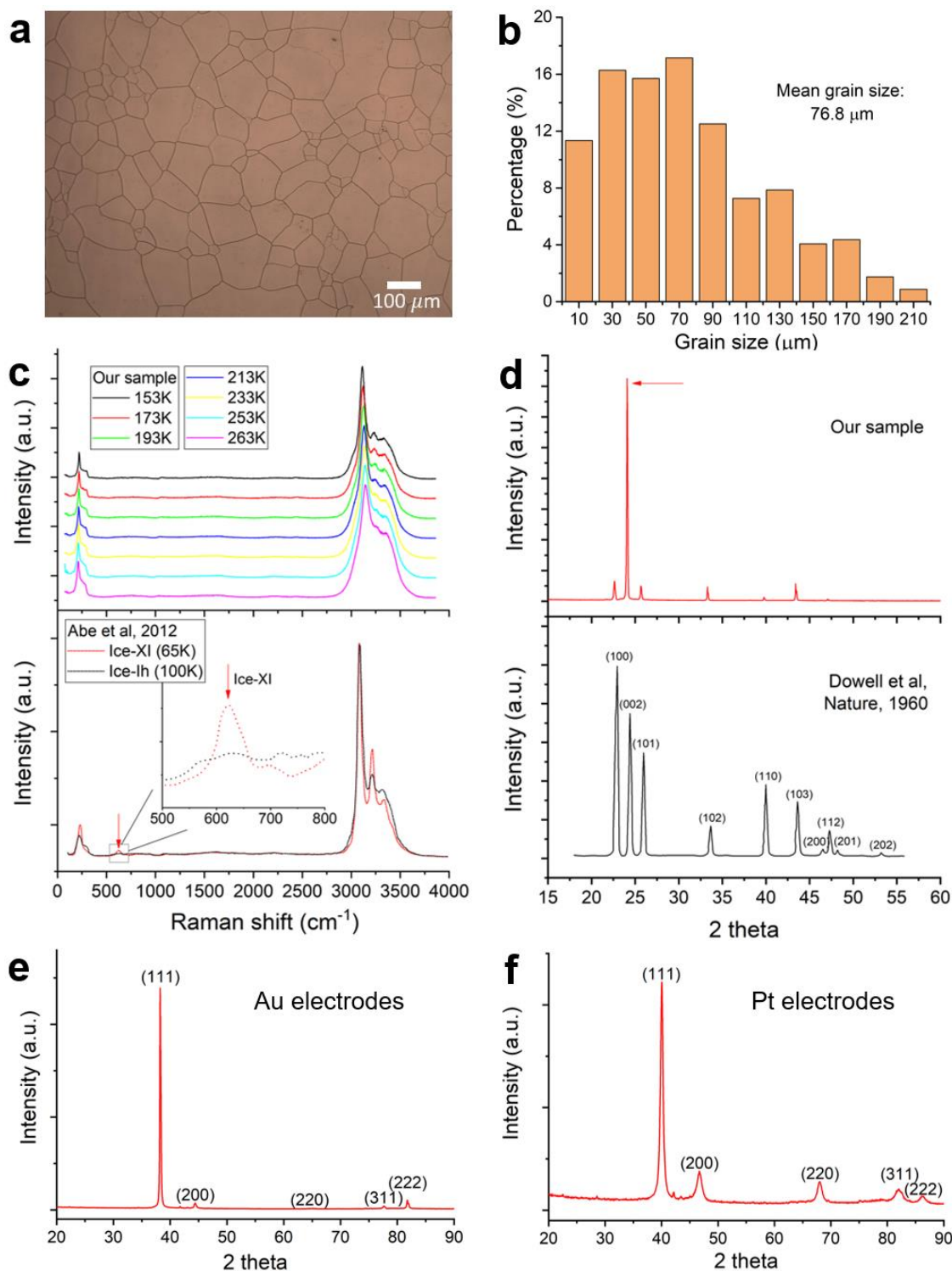


**Fig. S1.** Structural characterizations of our ice sample. **a**, Optical image of the sample surface. **b**, The statistical distribution of the grain size. **c**, The Raman spectrum measured at different temperatures, compared with the reported Raman spectrum for ice-Ih and ice-XI[105]. **d**, The X-ray diffraction pattern measured at 256 K, compared with the reported Xrd pattern for ice-Ih[106]. **e and f**, The X-ray diffraction pattern of Au and Pt electrodes respectively.

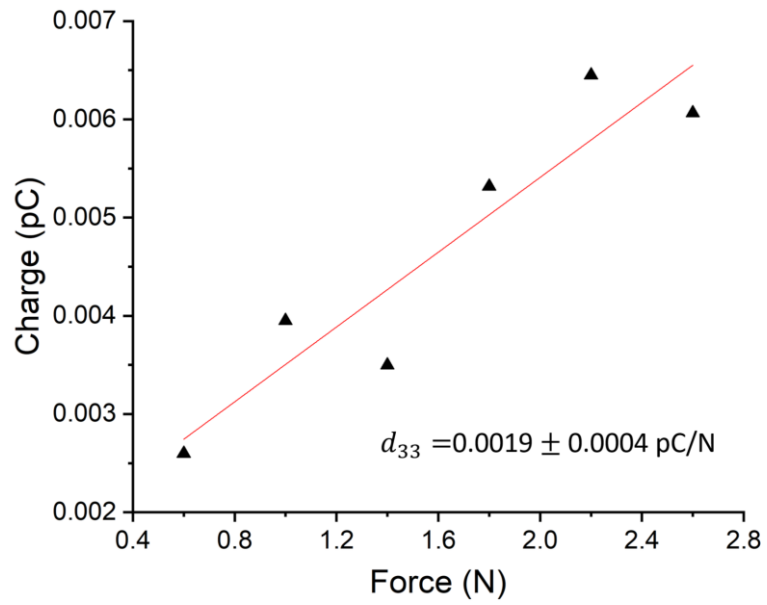


**Fig. S2.** Polarization charge versus the applied force in uniaxial compression experiments measured at  $\sim 233$  K

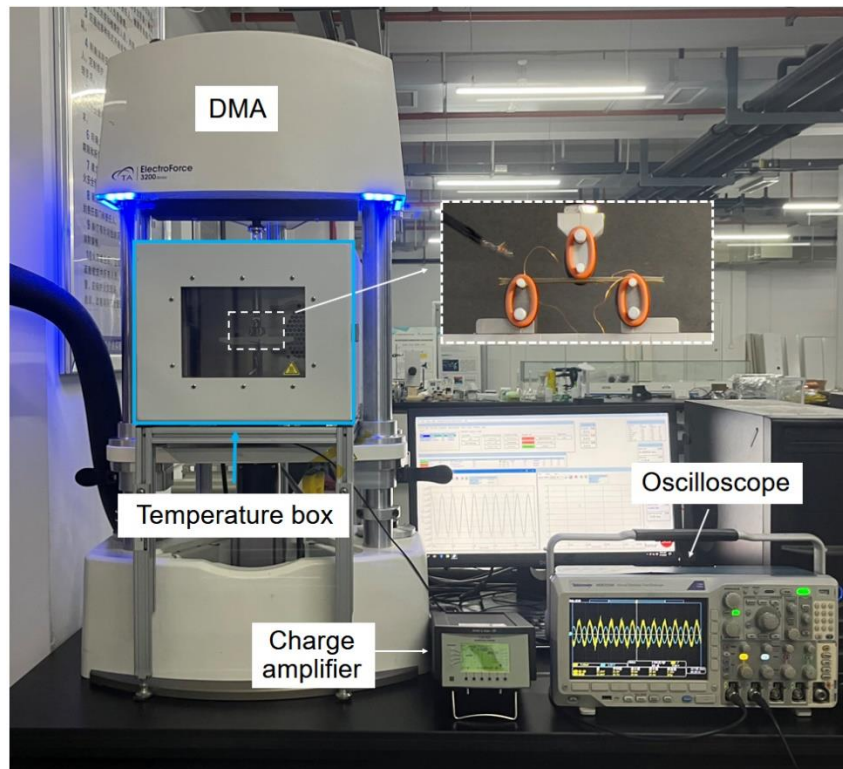


**Fig. S3.** Experimental setup, consisting of a dynamic mechanical analyzer (DMA) with temperature function, a charge amplifier, and an oscilloscope

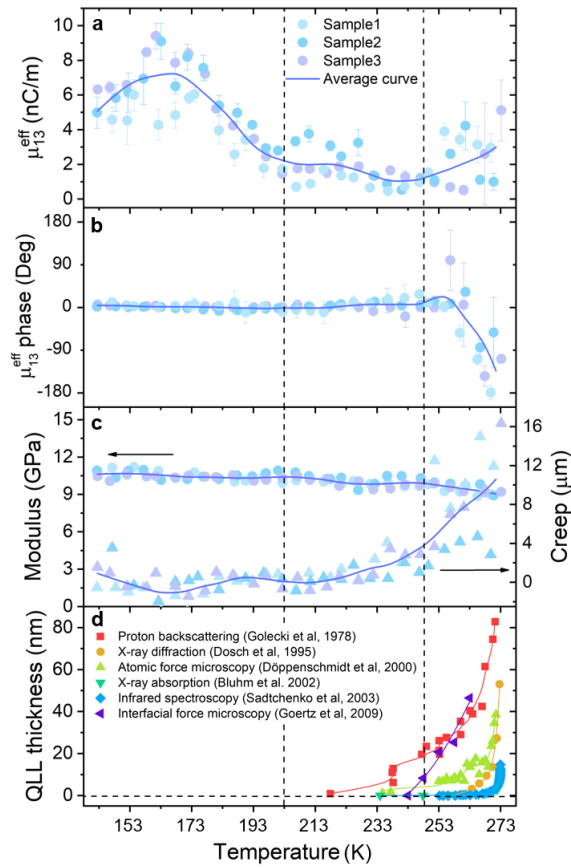


**Fig. S4.** **a**, The flexoelectric coefficient with Au electrodes versus temperature. **b**, The phase angle between displacement and polarization charge with Au electrodes versus temperature. **c**, The modulus and the creep displacement in the first ten seconds of loading versus temperature. **d**, The reported QLL thickness versus temperature measured with different techniques: X-ray absorption[19], Atomic force microscopy[20], Proton backscattering[21], X-ray diffraction[22], Infrared spectroscopy[23], Interfacial force microscopy[24].

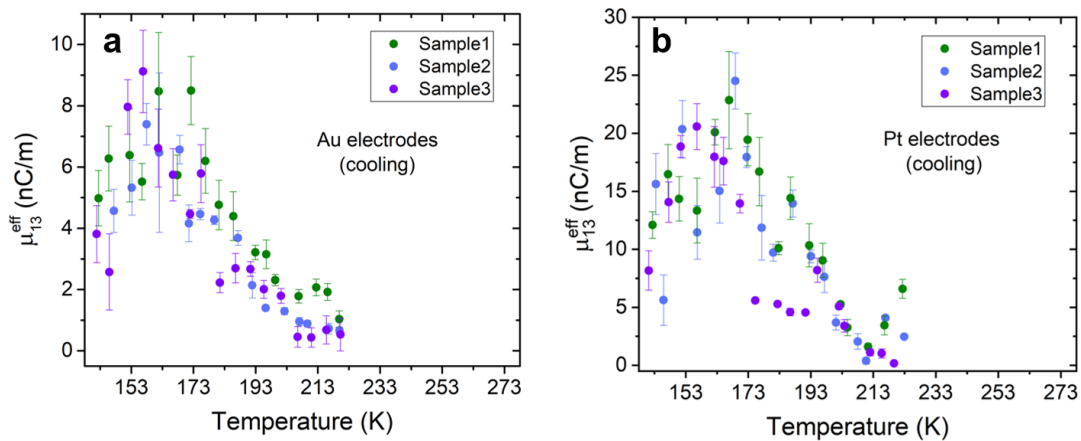


**Fig. S5.** The flexoelectric coefficient measured on cooling for samples with (a) Au electrodes and (b) Pt electrodes. The error bars represent the standard error from linear regressions.



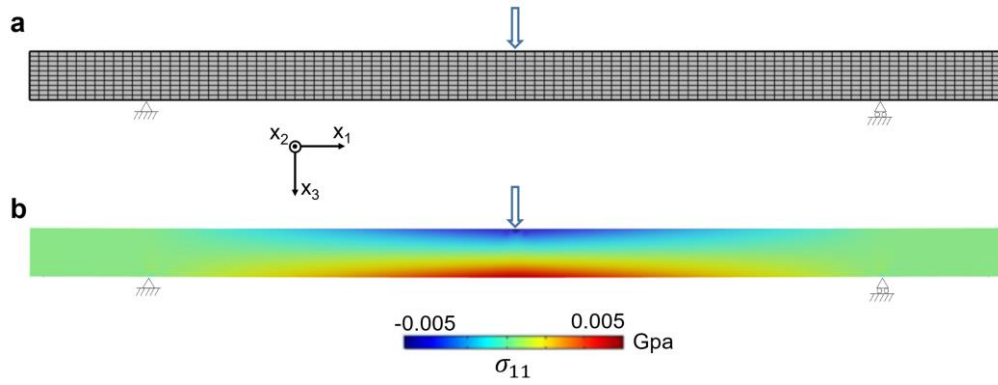


Fig. S6. Finite-element simulation of stress distribution in our sample under the maximum force (-2.5N).

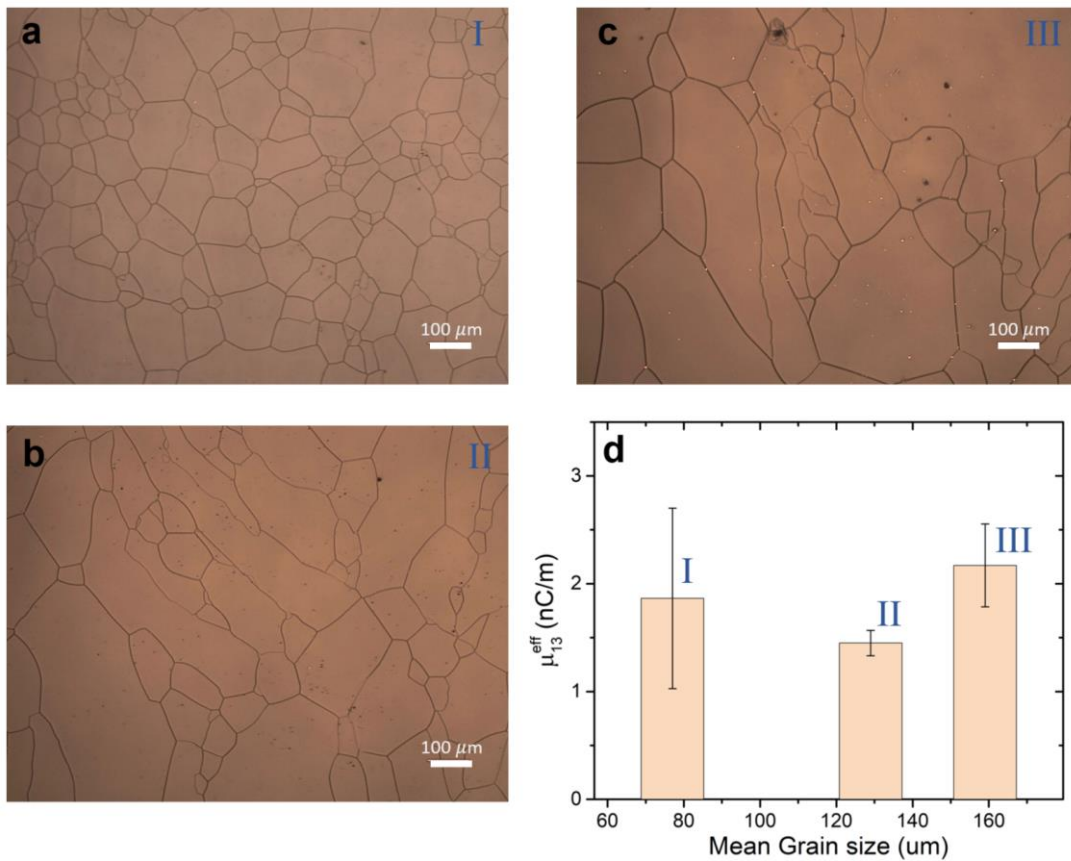


Fig. S7. Optical image of the grains on the surface of our ice sample (a) before annealing, (b) after annealing for half hour at 267 K and (c) after annealing for one hour at 267 K. d, The grain-size dependence of the flexoelectric coefficient measured at 233K.

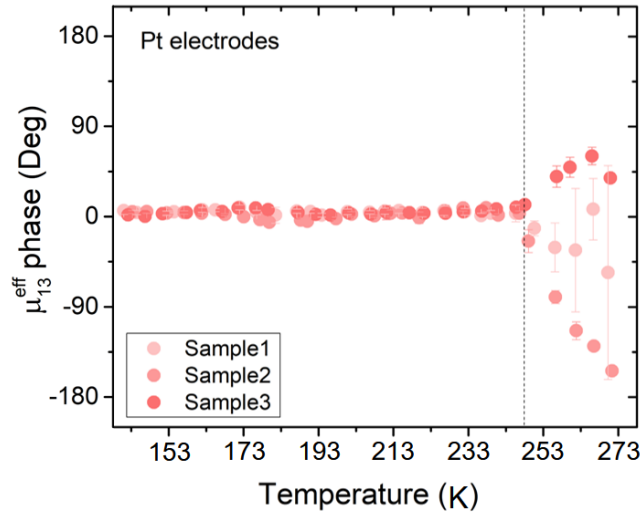


Fig. S8. The phase angle between displacement and charge measured in three ice samples with Pt electrodes on heating. The error bars represent the standard deviation from the average of multiple measurements.

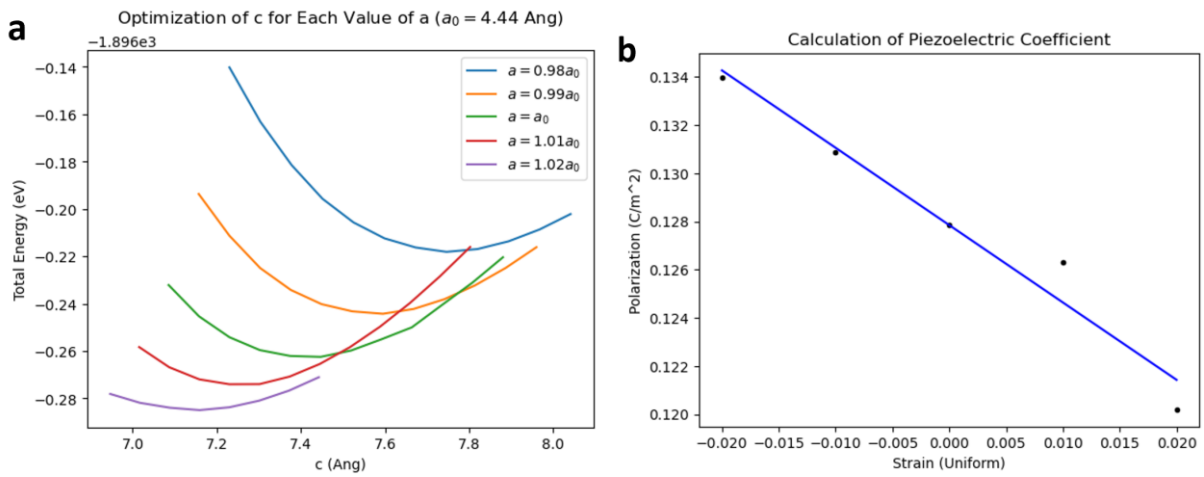


Fig. S9. Calculation of the transverse piezoelectric constant of ice XI.

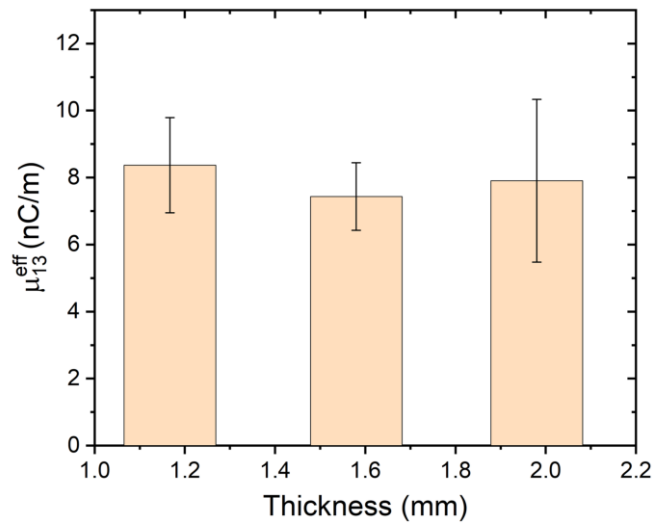


Fig. S10. Thickness dependence of  $\mu_{13}^{eff}$  for ice with Au electrodes measured at  $\sim 160\text{K}$ .

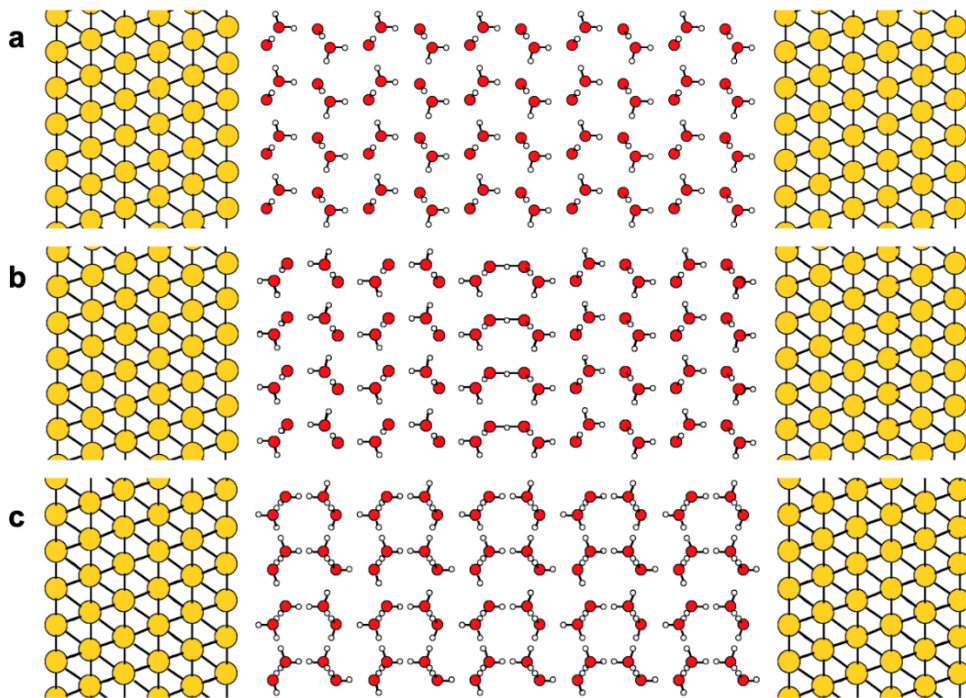
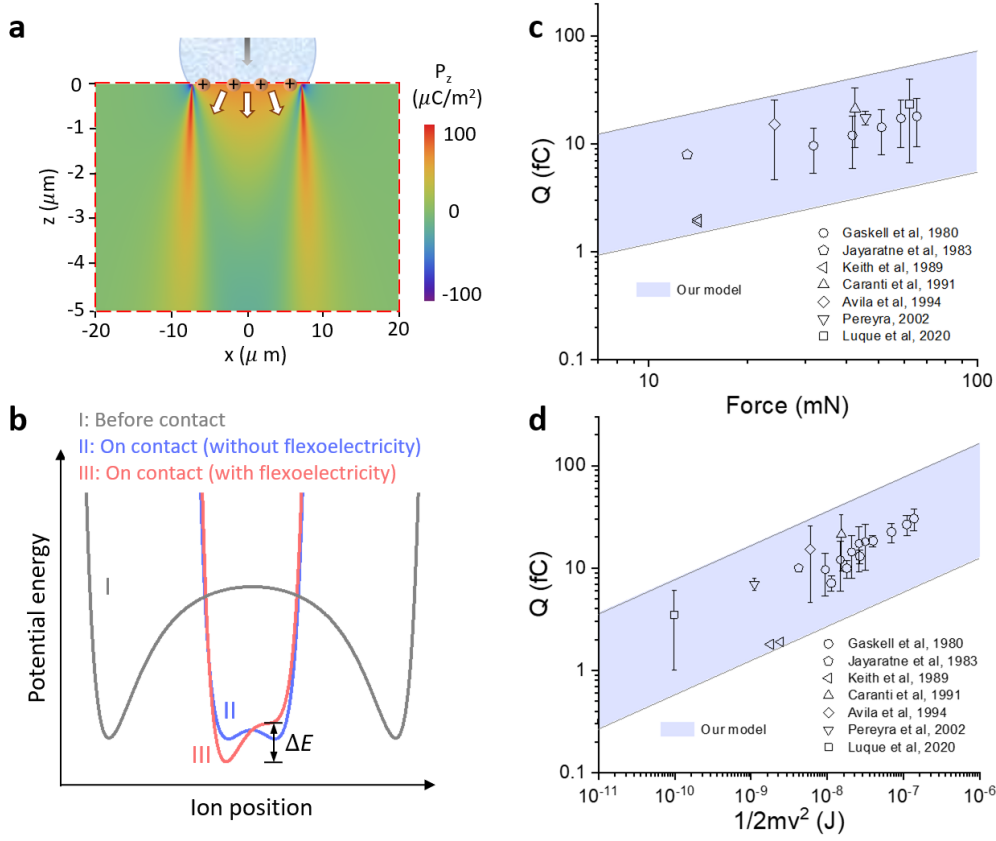


Fig. S11. Illustration of ice XI-Au interface with (a) one O-interface and one H-interface, and (b) two H-interfaces with a layer of defects in the middle. (c) Illustration of ice Ih-Au interface.



**Fig. S12.** (a) The calculated distribution of the vertical flexoelectric polarization beneath the indentation surface. (b) Schematic illustration of flexoelectricity facilitating charge transfer via altering the potential energy landscape of ions (adapted and revised from [41,43]) residing on ice surfaces. (c)  $Q$  versus  $F$  when  $R=50\mu\text{m}$ . (d)  $Q$  versus kinetic energy ( $\frac{1}{2}mv^2$ ). c and d show quantitative agreements between our calculations and the transferred charge reported in previous experiments [51-57,104].

$Y=Y_1$ (GPa)	$\nu=\nu_1=\nu_2$	$\xi_r$	$\mu$ (nC/m)
9.33[60]	0.325[60]	100[60]	2.1~8.0 (at 263K)
$R=R_1$ ( $\mu\text{m}$ )	$Y_2$ (GPa)	$\rho$ ( $\text{kg}/\text{m}^3$ )	$v_r$ (m/s)
10~300[72]	1~9[60,66,107]	916.7[60]	2~20[72]

**Table S1.** Parameters used in theoretical calculations.

- [1] T. Bartels-Rausch *et al.*, **84**, 885 (2012).
- [2] A. Garg, *physica status solidi (a)* **110**, 467 (1988).
- [3] O. Mishima, L. Calvert, and E. Whalley, *Nature* **310**, 393 (1984).
- [4] W. Ma and L. E. Cross, *Appl Phys Lett* **88**, 232902 (2006).
- [5] Z. Dai, S. Guo, Y. Gong, and Z. Wang, *Ceram Int* **47**, 6535 (2021).
- [6] P. Zubko, G. Catalan, A. Buckley, P. R. Welche, and J. F. Scott, *Phys Rev Lett* **99**, 167601 (2007).
- [7] J. Narvaez, S. Saremi, J. Hong, M. Stengel, and G. Catalan, *Phys Rev Lett* **115**, 037601 (2015).
- [8] P. Ordejón, E. Artacho, and J. M. Soler, *Physical review B* **53**, R10441 (1996).
- [9] J. M. Soler, E. Artacho, J. D. Gale, A. García, J. Junquera, P. Ordejón, and D. Sánchez-Portal, *Journal of Physics: Condensed Matter* **14**, 2745 (2002).
- [10] P. Zubko, G. Catalan, and A. K. Tagantsev, *Annual Review of Materials Research* **43**, 387 (2013).
- [11] A. K. Tagantsev and A. S. Yurkov, *J Appl Phys* **112** (2012).
- [12] L. Shu *et al.*, *Nat Mater* **19**, 605 (2020).
- [13] J. Narvaez, F. Vasquez-Sancho, and G. Catalan, *Nature* **538**, 219 (2016).
- [14] B. Pamuk, P. B. Allen, and M. V. Fernández-Serra, *Physical Review B* **92** (2015).
- [15] J. M. Ziman, *Principles of the Theory of Solids* (Cambridge university press, 1972).
- [16] L. Pauling, *Journal of the American Chemical Society* **57**, 2680 (1935).
- [17] W. Giaque and J. Stout, *Journal of the American Chemical Society* **58**, 1144 (1936).
- [18] W. F. Giaque and M. F. Ashley, *Physical review* **43**, 81 (1933).
- [19] H. Bluhm, D. F. Ogletree, C. S. Fadley, Z. Hussain, and M. Salmeron, *Journal of Physics: Condensed Matter* **14**, L227 (2002).
- [20] A. Döppenschmidt and H.-J. Butt, *Langmuir* **16**, 6709 (2000).
- [21] I. Golecki and C. Jaccard, *Journal of Physics C: Solid state physics* **11**, 4229 (1978).
- [22] H. Dosch, A. Lied, and J. Bilgram, *Surface science* **327**, 145 (1995).
- [23] V. Sadtchenko and G. E. Ewing, *Canadian journal of physics* **81**, 333 (2003).
- [24] M. Goertz, X.-Y. Zhu, and J. Houston, *Langmuir* **25**, 6905 (2009).
- [25] J. G. Dash, A. W. Rempel, and J. S. Wettlaufer, *Reviews of Modern Physics* **78**, 695 (2006).
- [26] J. Dash, H. Fu, and J. Wettlaufer, *Reports on Progress in Physics* **58**, 115 (1995).
- [27] B. Slater and A. Michaelides, *Nature Reviews Chemistry* **3**, 172 (2019).
- [28] H. Dosch, A. Lied, and J. H. Bilgram, *Surface science* **366**, 43 (1996).
- [29] V. F. Petrenko, *The Journal of Physical Chemistry B* **101**, 6276 (1997).
- [30] G.-J. Kroes, *Surface Science* **275**, 365 (1992).
- [31] E. Mazzega, U. del Pennino, A. Loria, and S. Mantovani, *The Journal of Chemical Physics* **64**, 1028 (1976).
- [32] A. Inagawa, M. Fukuyama, A. Hibara, M. Harada, and T. Okada, *Journal of colloid and interface science* **532**, 231 (2018).
- [33] A. Inagawa, M. Harada, and T. Okada, *The Journal of Physical Chemistry C* **123**, 6062 (2019).
- [34] J. Caranti and M. Lamfri, *Physics Letters A* **126**, 47 (1987).
- [35] N. Khusnatdinov, V. Petrenko, and C. Levey, *The Journal of Physical Chemistry B* **101**, 6212 (1997).
- [36] J. S. Wettlaufer and J. G. Dash, *Scientific American* **282**, 50 (2000).
- [37] G. Turner and C. Stow, *Philosophical Magazine A* **49**, L25 (1984).
- [38] G. J. Turner and C. Stow, *Journal of Geophysical Research: Atmospheres* **127**, e2021JD035552 (2022).
- [39] M. Baker and J. Dash, *Journal of Geophysical Research: Atmospheres* **99**, 10621 (1994).
- [40] E. Honegger and P. Henry, *Journal of the Textile Institute Proceedings* **48**, P5 (1957).

- [41] W. R. Harper, Oxford (1967).
- [42] J. Lowell and A. Rose-Innes, *Advances in Physics* **29**, 947 (1980).
- [43] L. S. McCarty and G. M. Whitesides, *Angewandte Chemie International Edition* **47**, 2188 (2008).
- [44] S. Pence, V. Novotny, and A. Diaz, *Langmuir* **10**, 592 (1994).
- [45] Y. Zhang, T. Pächtz, Y. Liu, X. Wang, R. Zhang, Y. Shen, R. Ji, and B. Cai, *Physical Review X* **5**, 011002 (2015).
- [46] H. Zhang, S. Sundaresan, and M. A. Webb, *Nature Communications* **15**, 2616 (2024).
- [47] J. Latham and B. J. Mason, *Proceedings of the Royal Society of London. Series A. Mathematical and Physical Sciences* **260**, 523 (1961).
- [48] P. Henry, *British Journal of Applied Physics* **4**, S31 (1953).
- [49] T. Pächtz, H. J. Herrmann, and T. Shinbrot, *Nature Physics* **6**, 364 (2010).
- [50] A. Illingworth and J. Caranti, *Journal of Geophysical Research: Atmospheres* **90**, 6033 (1985).
- [51] W. Gaskell and A. Illingworth, *Quarterly Journal of the Royal Meteorological Society* **106**, 841 (1980).
- [52] E. Jayaratne, C. Saunders, and J. Hallett, *Quarterly Journal of the Royal Meteorological Society* **109**, 609 (1983).
- [53] W. Keith and C. Saunders, *Meteorology and Atmospheric Physics* **41**, 55 (1989).
- [54] G. Caranti, E. Avila, and M. Ré, *Journal of Geophysical Research: Atmospheres* **96**, 15365 (1991).
- [55] E. E. Avila and G. M. Caranti, *Journal of Geophysical Research: Atmospheres* **99**, 10611 (1994).
- [56] M. Y. Luque, F. Nollas, R. G. Pereyra, R. E. Bürgesser, and E. E. Ávila, *Journal of Geophysical Research: Atmospheres* **125**, e2019JD030941 (2020).
- [57] R. G. Pereyra and E. E. Avila, *Journal of Geophysical Research: Atmospheres* **107**, AAC 23 (2002).
- [58] H. Lu, C. W. Bark, D. Esque de los Ojos, J. Alcalá, C. B. Eom, G. Catalan, and A. Gruverman, *Science* **336**, 59 (2012).
- [59] G. Catalan *et al.*, *Nat Mater* **10**, 963 (2011).
- [60] V. F. Petrenko and R. W. Whitworth, *Physics of ice* (OUP Oxford, 1999).
- [61] D. J. Lacks and T. Shinbrot, *Nature Reviews Chemistry* **3**, 465 (2019).
- [62] D. M. Wood, *Phys Rev Lett* **46**, 749 (1981).
- [63] D. J. Lacks and R. M. Sankaran, *Journal of Physics D: Applied Physics* **44**, 453001 (2011).
- [64] E. Workman and S. Reynolds, *Physical Review* **78**, 254 (1950).
- [65] E. Workman and S. Reynolds, *Physical Review* **74**, 709 (1948).
- [66] C. J. P. A. E. Saunders, 335 (2008).
- [67] J. Caranti and A. Illingworth, *Journal of Geophysical Research: Oceans* **88**, 8483 (1983).
- [68] G. W. Gross, *Journal of Geophysical Research: Oceans* **87**, 7170 (1982).
- [69] B. J. Mason, *Proceedings of the Royal Society of London. A. Mathematical and Physical Sciences* **415**, 303 (1988).
- [70] E. E. Avila, G. G. A. Varela, and G. M. Caranti, *Journal of Atmospheric Sciences* **52**, 4515 (1995).
- [71] W. Gaskell, *Quarterly Journal of the Royal Meteorological Society* **107**, 955 (1981).
- [72] T. Takahashi, *Journal of Atmospheric Sciences* **35**, 1536 (1978).
- [73] S. Reynolds, M. Brook, and M. F. Gourley, *Journal of Atmospheric Sciences* **14**, 426 (1957).
- [74] T. Takahashi, *Journal of the Meteorological Society of Japan. Ser. II* **47**, 23 (1969).
- [75] J. Latham, *British Journal of Applied Physics* **14**, 488 (1963).
- [76] C. Emersic and C. Saunders, *Atmospheric Research* **98**, 327 (2010).
- [77] B. Baker, M. Baker, E. Jayaratne, J. Latham, and C. Saunders, *Quarterly Journal of the Royal Meteorological Society* **113**, 1193 (1987).

- [78] J. Dash, B. Mason, and J. Wettlaufer, *Journal of Geophysical Research: Atmospheres* **106**, 20395 (2001).
- [79] B. Mason and J. Dash, *Journal of Geophysical Research: Atmospheres* **105**, 10185 (2000).
- [80] C. Emersic and C. Saunders, *Atmospheric research* **242**, 104962 (2020).
- [81] M. M. Apodaca, P. J. Wesson, K. J. Bishop, M. A. Ratner, and B. A. Grzybowski, *Angewandte Chemie International Edition* **5**, 946 (2010).
- [82] H. Baytekin, A. Patashinski, M. Branicki, B. Baytekin, S. Soh, and B. A. Grzybowski, *Science* **333**, 308 (2011).
- [83] G. Fatti *et al.*, *Phys Rev Lett* **131**, 166201 (2023).
- [84] Y. Fang, C. K. Ao, Y. Jiang, Y. Sun, L. Chen, and S. Soh, *Nature Communications* **15**, 1986 (2024).
- [85] F. Vasquez-Sancho, A. Abdollahi, D. Damjanovic, and G. Catalan, *Adv Mater* **30**, 1705316 (2018).
- [86] K. Cordero-Edwards, H. Kianirad, C. Canalias, J. Sort, and G. Catalan, *Phys Rev Lett* **122**, 135502 (2019).
- [87] P. Gao, S. Yang, R. Ishikawa, N. Li, B. Feng, A. Kumamoto, N. Shibata, P. Yu, and Y. Ikuhara, *Phys Rev Lett* **120**, 267601 (2018).
- [88] H. Wang, X. Jiang, Y. Wang, R. W. Stark, P. A. van Aken, J. Mannhart, and H. Boschker, *Nano Lett* **20**, 88 (2019).
- [89] Y. Du, S. Zhang, and Z. Cheng, *Nano Energy*, 109731 (2024).
- [90] G. Zhang, F. Deng, W. Liu, and S. Shen, *J Phys D* **55**, 315302 (2022).
- [91] P. Y. Wu, K. T. Le, H.-Y. Lin, Y.-C. Chen, P.-H. Wu, and J. M. Wu, *ACS nano* **17**, 17417 (2023).
- [92] T. Wu, K. Liu, S. Liu, X. Feng, X. Wang, L. Wang, Y. Qin, and Z. L. Wang, *Advanced Materials* **35**, 2208121 (2023).
- [93] S. Cho *et al.*, *Nature Communications* **15**, 387 (2024).
- [94] H. Kang, R. Jayaratne, and E. Williams, *Journal of Geophysical Research: Atmospheres*, e2023JD038626 (2023).
- [95] P. Zubko, G. Catalan, and A. K. Tagantsev, *Annu Rev Mater Sci* **43**, 387 (2013).
- [96] P. V. Yudin and A. K. Tagantsev, *Nanotechnology* **24**, 432001 (2013).
- [97] J. Očenášek, H. Lu, C. Bark, C.-B. Eom, J. Alcalá, G. Catalan, and A. Gruverman, *Phys Rev B* **92**, 035417 (2015).
- [98] B. Wang, H. Lu, C. W. Bark, C.-B. Eom, A. Gruverman, and L.-Q. Chen, *Acta Materialia* **193**, 151 (2020).
- [99] A. C. Fischer-Cripps, *Introduction to contact mechanics* (Springer, 2007), Vol. 101.
- [100] S. M. Park, B. Wang, L.-Q. Chen, T. W. Noh, S. M. Yang, and D. Lee, *Appl Phys Rev* **8**, 041327 (2021).
- [101] C. A. Mizzi, A. Y. W. Lin, and L. D. Marks, *Phys Rev Lett* **123**, 116103 (2019).
- [102] M. M. Yang, D. J. Kim, and M. Alexe, *Science* **360**, 904 (2018).
- [103] K. L. Johnson, *Contact mechanics* (Cambridge university press, 1987).
- [104] W. Gaskell, *Field and laboratory studies of precipitation charges* (The University of Manchester (United Kingdom), 1979).
- [105] T. Shigenari and K. Abe, *The Journal of Chemical Physics* **136** (2012).
- [106] L. G. Dowell and A. P. Rinfret, *Nature* **188**, 1144 (1960).
- [107] A. J. Heymsfield, (2003).